Redox interconversion between metal thiolate and disulfide compounds

Jiang, F.

Appendix I

Supplementary information on Chapter 2

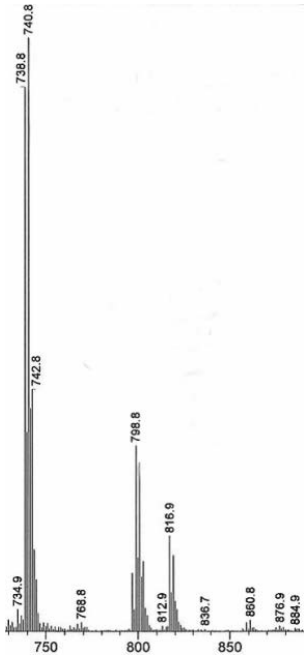

Figure AI.1. ESI-MS spectrum of compound $\mathbf{1}_{Co}$ dissolved in acetonitrile. ESI-MS found (calcd) for $[M-Cl]^+$ *m/z* 740.8 (740.9); for $[M-Cl+MeCN+H_2O]^+$ *m/z* 798.1 (798.8).

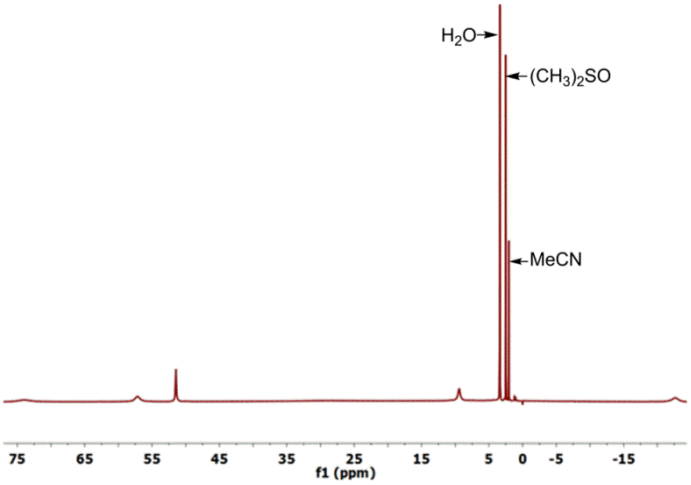

Figure AI.2. ^{1}H NMR spectrum of compound $\mathbf{1_{Co}}$ dissolved in dimethyl sulfoxide-d_6.

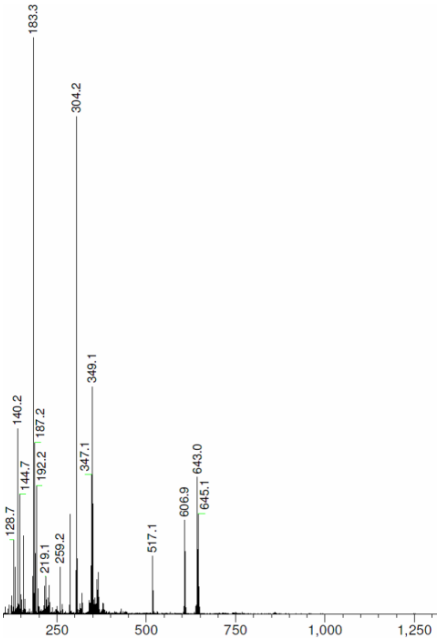

Figuare AI.3. ESI-MS spectrum of Fe^{II} disulfide compound $\mathbf{1_{Fe}}$ dissolved in methanol. ESI-MS found (calcd) for ¼$[Fe^{II}_2(L^1SSO_2L^1)\cdot 4H_2O]^{4+}$, *m/z* 183.3 (183.1), ½$[Fe^{II}(L^1SSL^1)\cdot 2H_2O]^{2+}$, *m/z* 304.2 (304.1) ½$[Fe^{II}_2(L^1SSL^1)Cl_2]^{2+}$ *m/z* 349.1 (349.0), $[L^1SSL^1+H]^+$ *m/z* 517.1 (517.2), $[Fe^{II}(L^1SSL^1)Cl_2 + H]^+$ *m/z* 643.0 (643.1).

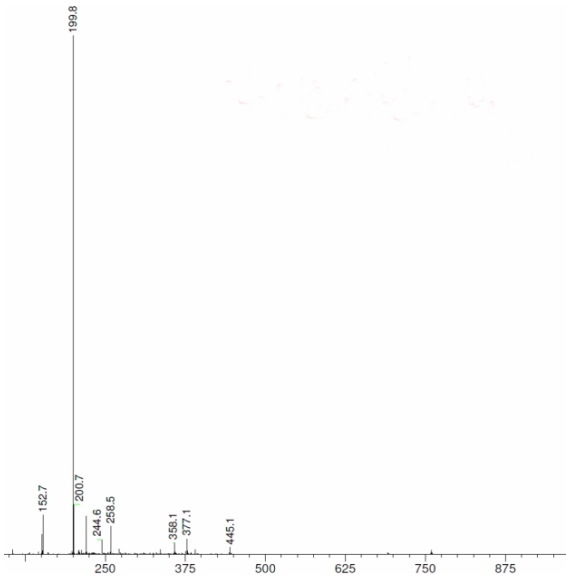

Figure AI.4. ESI-MS spectrum of compound **2** dissolved in acetonitrile. ESI-MS found (calcd) for ½[M−2(BF_4)+2MeCN]$^{2+}$ *m/z* 199.8 (199.5).

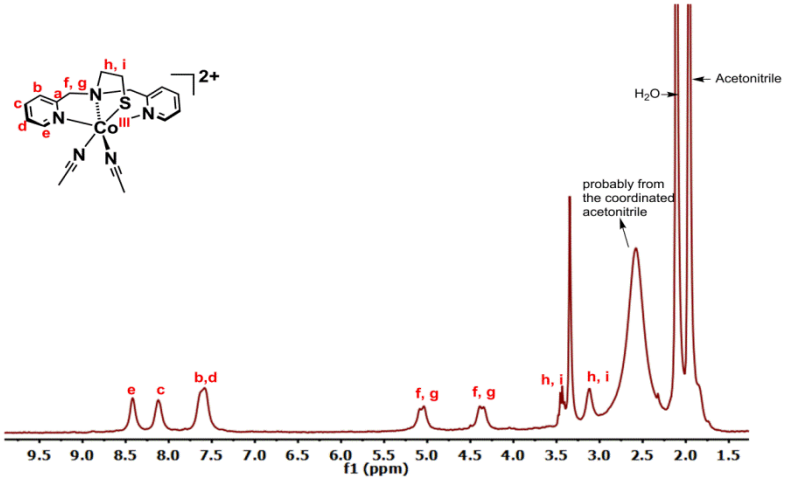

Figure AI.5. ^{1}H NMR spectrum of compound **2** dissolved in acetonitrile-d_3.

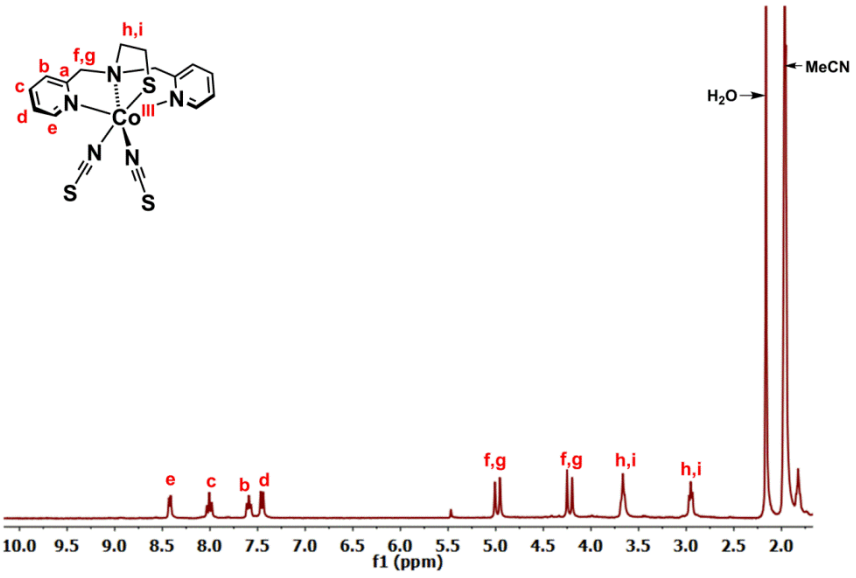

Figure AI.6. ^{1}H NMR spectrum of compound **3** dissolved in acetonitrile-d_3.

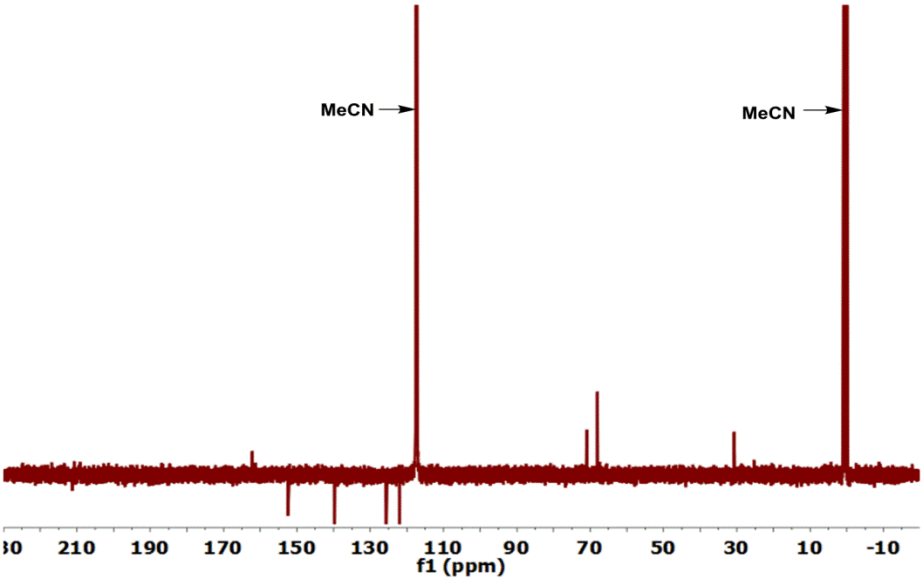

Figure AI.7. ^{13}C NMR spectrum of compound **3** dissolved in acetonitrile-d_3.

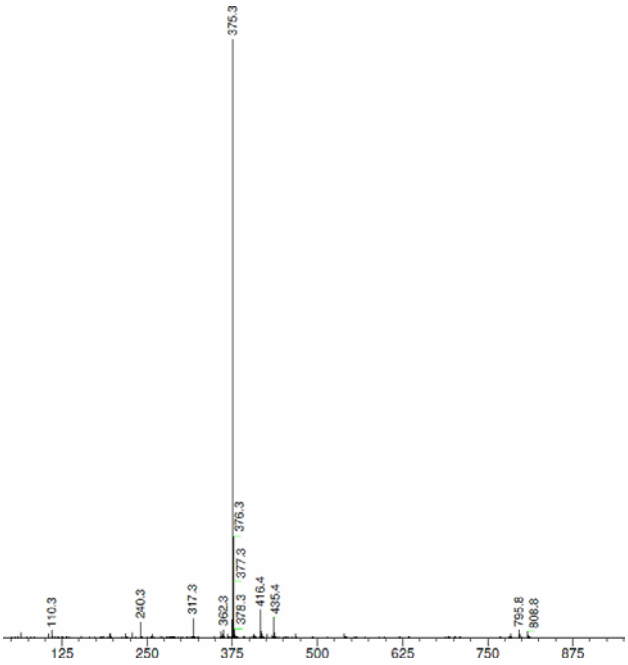

Figure AI.8. ESI-MS spectrum of compound **3** dissolved in acetonitrile. ESI-MS found (calcd) for $[M-NCS]^+$ *m/z* 375.3 (375.4).

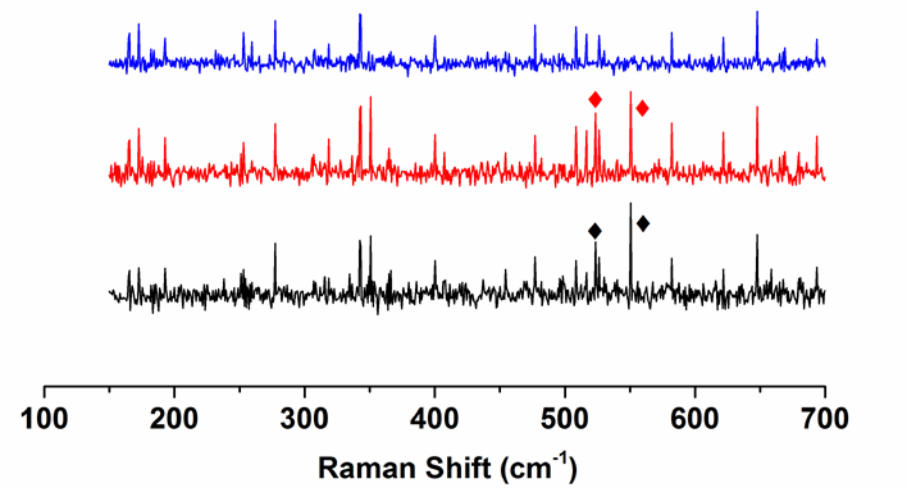

Figure AI.9. Raman spectra of ligand L^1SSL^1(black line), compounds $\mathbf{1}_{Co}$ (red line), and **2** (blue line). The diamonds represent the peaks arising from the S–S bond vibration.

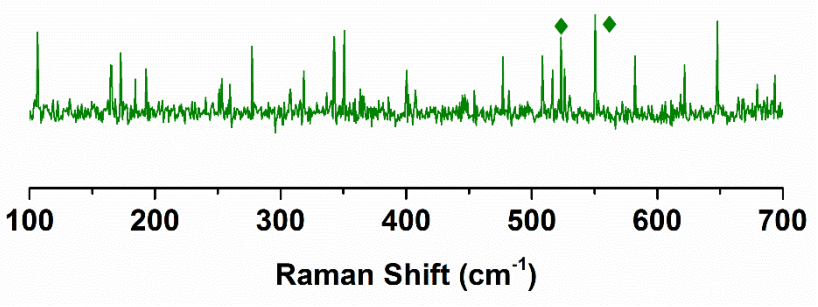

Figure AI.10. Raman spectra of compound $\mathbf{1}_{Fe}$. The diamonds represent the peaks arising from the S–S bond vibration.

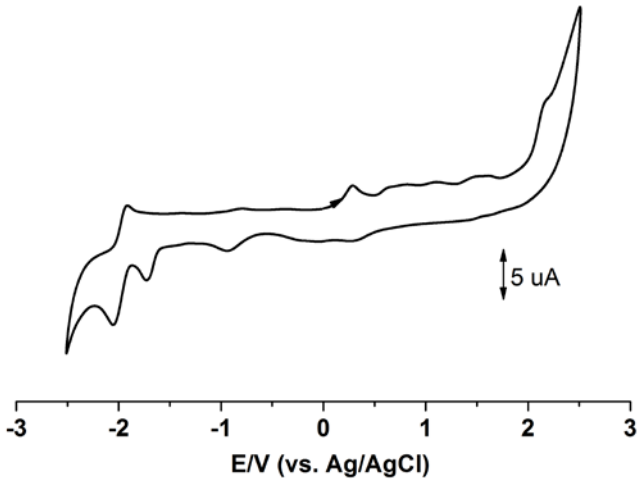

Figure AI.11. The cyclic voltammograms of compound $\mathbf{1}_{Co}$ (1 mM) in an acetonitrile solution containing 0.1 M NBu_4PF_6 as the supporting electrolyte and using a glassy carbon electrode at a scan rate of 100 mV s^{-1}. The potential is given vs. Ag/AgCl.

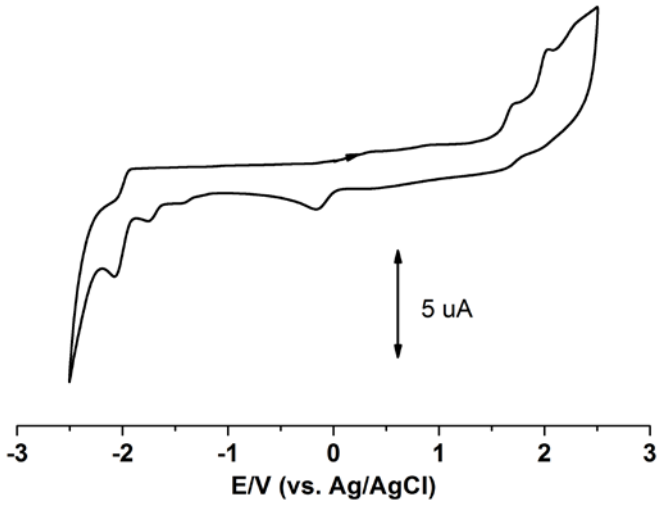

Figure AI.12. The cyclic voltammograms of compound **2** (2 mM) in an acetonitrile solution containing 0.1 M $TBAPF_6$ as the supporting electrolyte and using a glassy carbon electrode at a scan rate of 100 mV s^{-1}. The potential is given vs. Ag/AgCl.

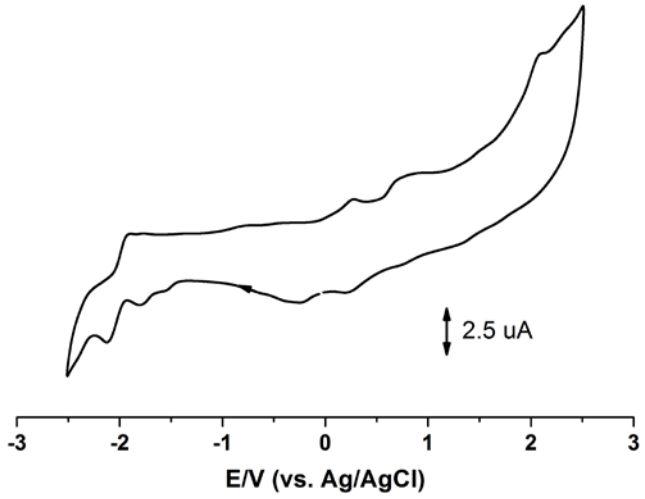

Figure AI.13. The cyclic voltammograms of compound **3** (2 mM) in an acetonitrile solution containing 0.1 M NBu_4PF_6 as the supporting electrolyte and using a glassy carbon electrode at a scan rate of 100 mV s^{-1}. The potential is given vs. Ag/AgCl.

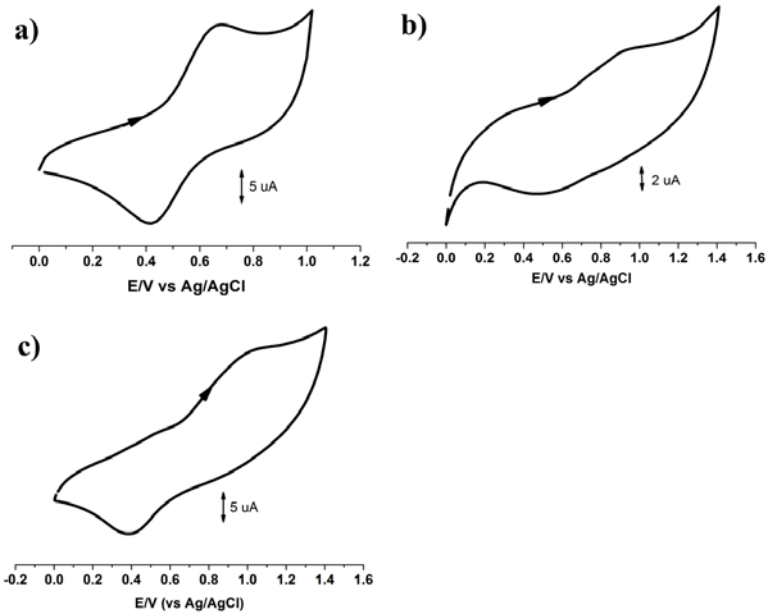

Figure AI.14. The cyclic voltammograms of (a) compound $\mathbf{1}_{Co}$ (1 mM), (b) compound **2** (2 mM), and (c) compound **3** (2 mM) in an acetonitrile solution containing 0.1 M NBu_4PF_6 as the supporting electrolyte and using a glassy carbon electrode at a scan rate of 100 mV s^{-1}. Potentials are given vs. Ag/AgCl.

Table AI.1. Crystallographic and structure refinement data of compounds $\mathbf{1_{Co}}$, $\mathbf{2_{Ox}}$, **3** and $\mathbf{1_{Fe}}$.

	$\mathbf{1_{Co}}$	$\mathbf{2_{Ox}}$	**3**	$\mathbf{1_{Fe}}$
Chemical formula	$C_{28}H_{32}Cl_4Co_2N_6S_2 \cdot C_4H_{10}O$	$C_{18}H_{22}CoN_5O_2S \cdot 2(BF_4) \cdot 2(C_2H_3N)$	$C_{16}H_{16}CoN_5O_{0.18}S_3$	$C_{28}H_{32}Cl_4Co_2N_6S_2 \cdot 2(CH_4O)$
Formula Weight	850.49	687.12	436.33	834.30
Crystal system, space group	Triclinic, *P*–1	Triclinic, *P*–1	Orthorhombic, *Pbca*	Monoclinic, *Cc*
Temperature (K)	110	110	110	110
a, *b*, *c* (Å)	8.2673(2), 13.6866(4), 17.1779(7)	11.7231 (3), 13.1844 (3), 20.0200 (6)	11.0351(2), 16.5646(3), 19.6200(4)	28.6815(7), 9.11583(17), 15.3360(4)
α, β, γ (°)	90.875(3), 102.152(3), 92.315(2)	70.877 (2), 86.502 (2), 81.384 (2)	90, 90, 90	90, 116.791(3), 90
V (Å^3)	1898.03(11)	2890.35 (14)	3586.38(12)	3579.27(17)
Z	2	4	8	4
Radiation type	Mo *K*α	Mo *K*α	Mo *K*α	Mo *K*α
μ (mm^{-1})	1.30	0.753	1.32	1.264
Crystal size (mm)	0.35 × 0.24 × 0.07	0.37 × 0.13 × 0.06	0.28 × 0.21 × 0.13	0.31 × 0.24 × 0.17
Diffractometer	SuperNova, Dual, Cu at zero, Atlas	SuperNova, Dual, Cu at zero, Atlas	SuperNova, Dual, Cu at zero, Atlas	SuperNova, Dual, Cu at zero, Atlas
T_{min}, T_{max}	0.755, 0.925	0.561, 1.000	0.436, 1.000	0.556, 0.729
No. of measured, independent and observed [$I > 2\sigma(I)$] reflections	29644, 8726, 6714	41812, 13267, 10130	52080, 4121, 3755	26618, 7654, 7433
R_{int}	0.047	0.040	0.036	0.0291
$(\sin\theta/\lambda)_{max}$ (Å^{-1})	0.650	0.650	0.650	0.650
$R[F^2 > 2\sigma(F^2)]$, $wR(F^2)$, *S*	0.040, 0.089, 1.03	0.043, 0.105, 1.04	0.028, 0.070, 1.09	0.022, 0.049, 1.03
No. of reflections	8726	13267	4121	7654
No. of parameters	426	817	236	423
H-atom treatment	H-atom parameters constrained	H-atom parameters constrained	H-atom parameters constrained	H-atom parameters constrained
$\Delta\rho_{max}$, $\Delta\rho_{min}$ (e Å^{-3})	0.83, –1.00	0.71, –0.46	0.85, –0.59	0.31, –0.20

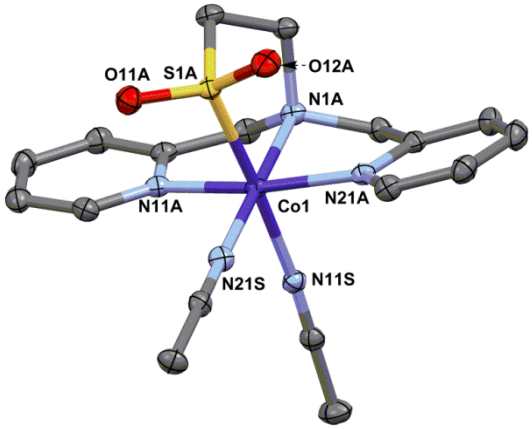

Figure AI.15. Displacement ellipsoid plot (50% probability level) of the cationic part of cobalt(III) sulfinate compound $\mathbf{2_{Ox}}$.

Table AI.2. Selected bond distances (Å) and angles (°) for the crystal structure of compound $[Co^{III}(L^1SO_2)(MeCN)_2](BF_4)_2$ ($\mathbf{2_{Ox}}$).

Distance (Å)			
Co1–N1A	1.9494(19)	Co1–S1A	2.1837(6)
Co1–N11A	1.944(2)	Co1–N11S	2.010(2)
Co1–N21A	1.9384(19)	Co1–N21S	1.916(2)
Angles (°)			
N21S–Co1–N21A	95.38(8)	N11A–Co1–N11S	88.97(8)
N21S–Co1–N11A	96.49(8)	N1A–Co1–N11S	92.38(8)
N21A–Co1–N11A	168.11(8)	N21S–Co1–S1A	89.34(6)
N21S–Co1–N1A	179.06(8)	N21A–Co1–S1A	87.55(6)
N21A–Co1–N1A	85.13(8)	N11A–Co1–S1A	93.23(6)
N11A–Co1–N1A	83.01(8)	N1A–Co1–S1A	89.89(6)
N21S–Co1–N11S	88.40(8)	N11S–Co1–S1A	177.01(6)
N21A–Co1–N11S	90.72(8)		

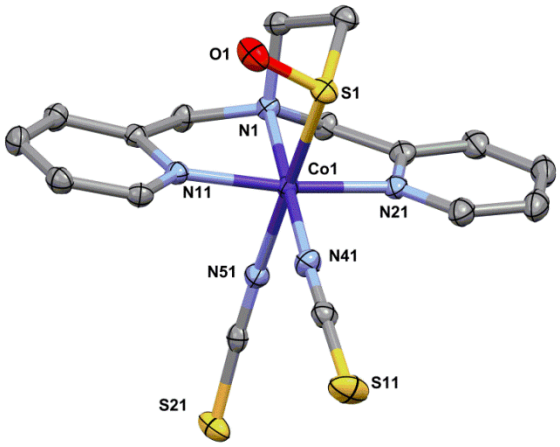

Figure AI.16. Displacement ellipsoid plot (50% probability level) of the oxidized part of the compound **3** present with an occupancy factor of 0.178(5) at 110(2) K. All hydrogen atoms are omitted for clarity.

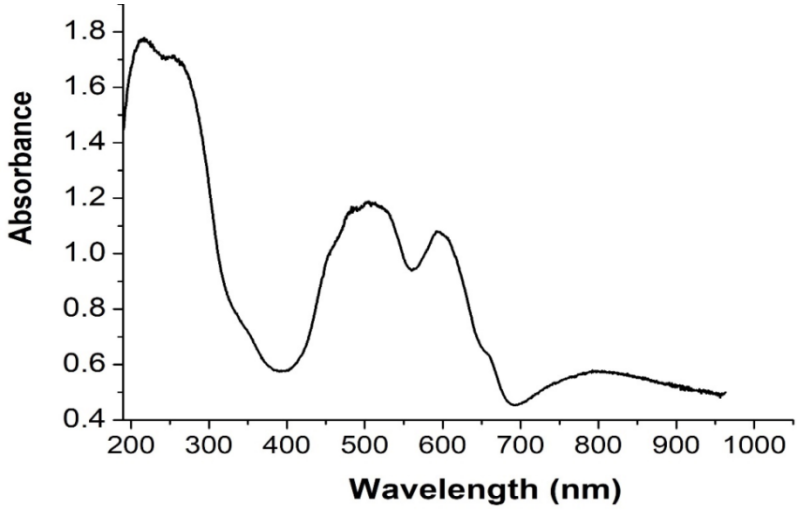

Figure AI.17. UV-vis spectrum of compound $\mathbf{1_{Co}}$ in the solid state.

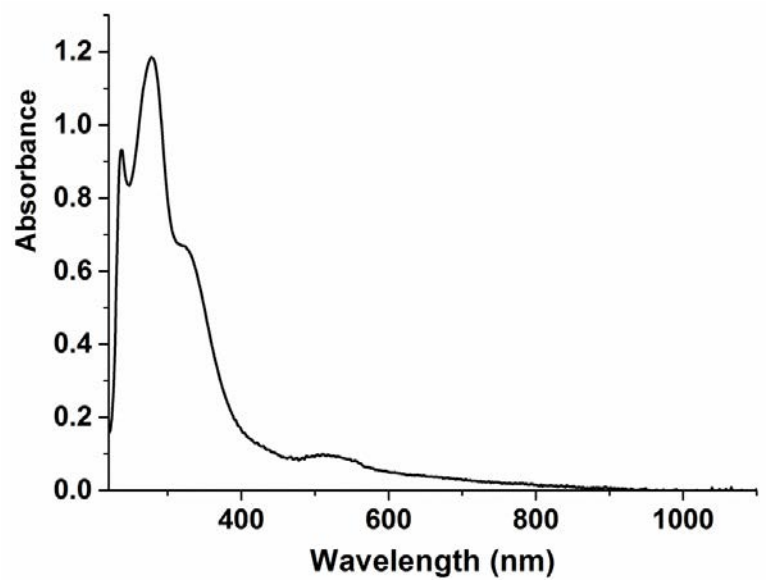

Figure AI.18. UV-vis spectrum of compound **3** dissolved in acetonitrile. UV-vis spectra were recorded using solutions 1 mM in [Co] with a transmission dip probe path length of 1.4 mm.

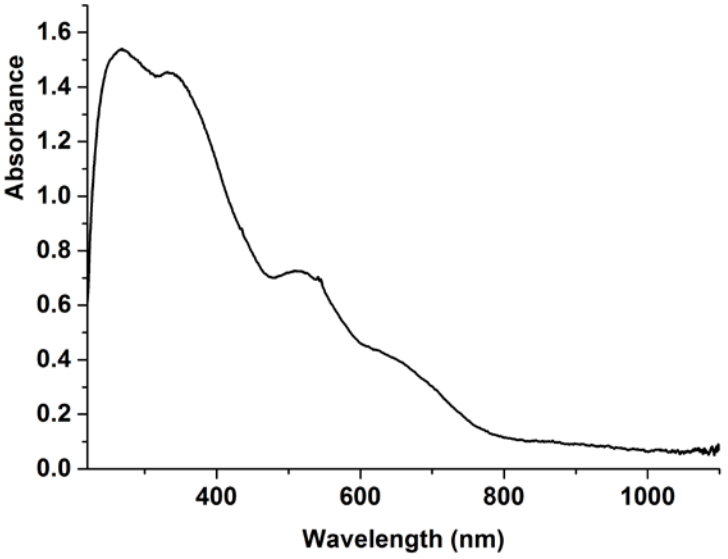

Figure AI.19. UV-vis spectrum of compound **3** in solid state.

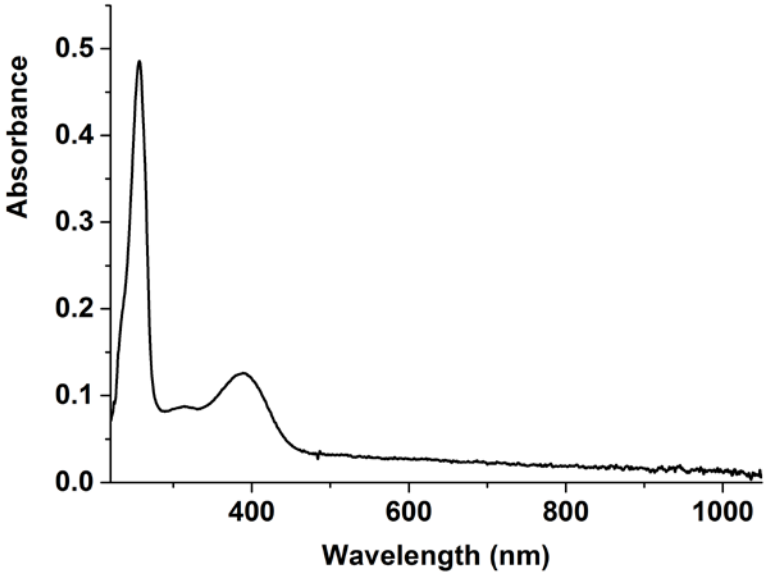

Figure AI.20. UV-vis spectrum of compound $\mathbf{1}_{Fe}$ dissolved in methanol. UV-vis spectra were recorded using solutions 1 mM in [Fe] with a transmission dip probe path length of 1.2 mm.

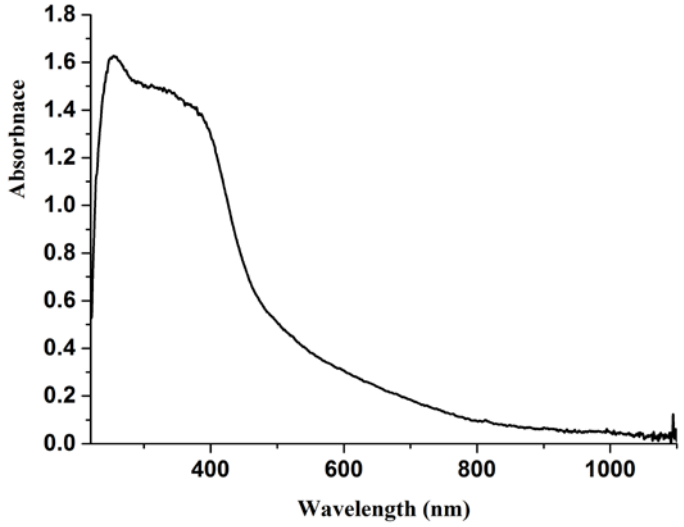

Figure AI.21. UV-vis spectrum of the compound $\mathbf{1}_{Fe}$ in solid state.

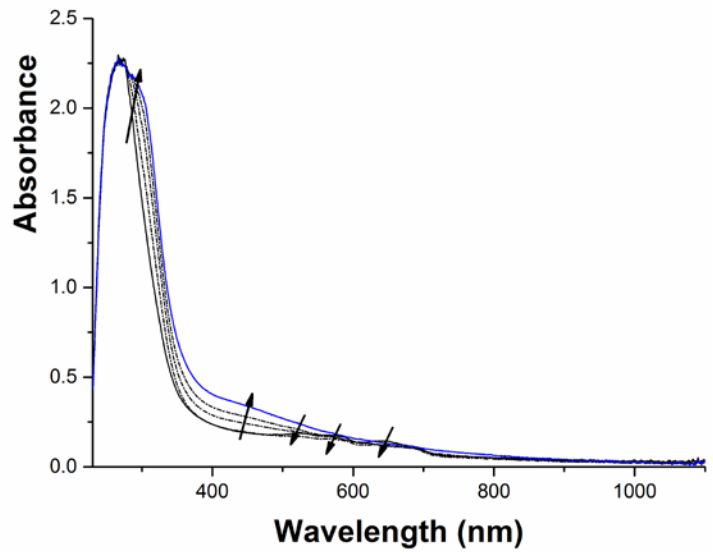

Figure AI.22. UV-vis spectra recorded upon addition of $AgBF_4$ to a solution of the compound $\mathbf{1}_{Co}$. The spectra were recorded in at a concentration of 5 mM [Co] with a transmission dip probe path length of 1.8 mm.

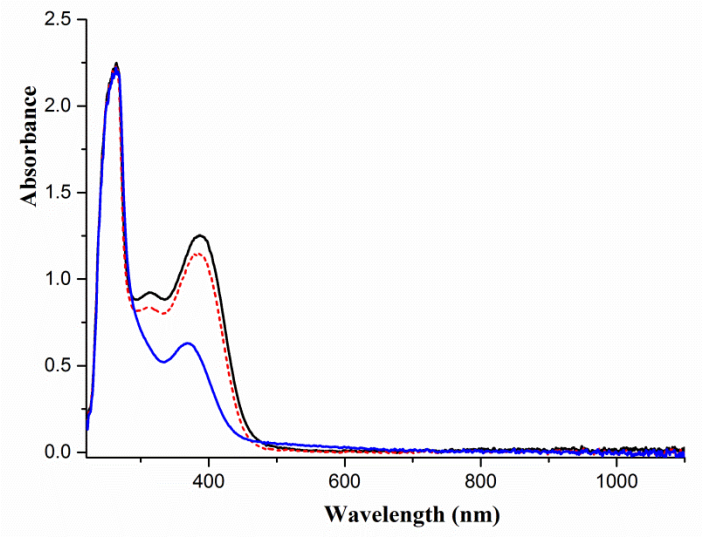

Figure AI.23. UV-vis spectra recorded upon addition of 2 equiv. (red dotted line), and 4 equiv. (blue line) $AgBF_4$ to a solution of the compound $\mathbf{1}_{Fe}$. The spectra were recorded in at a concentration of 2 mM [Fe] with a transmission dip probe path length of 2.2 mm.

Table AI.3. The total energies (kcal/mol) of the compound $\mathbf{1_{Co}}$ in the gas phase and in acetonitrile with different spin states (S = 1/2, 3/2).

$\mathbf{1_{Co}}$	S = 3/2	S = 1/2
Energy(gas)	-10456	-10440
Gibbs energy(gas)	-10153	-10133
Energy(solvated)	-10496	-10488
Gibbs energy(solvated)	-10194	-10181

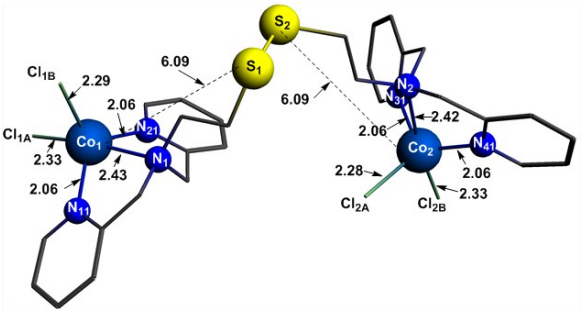

Figure AI.24. The optimized structure of the compound $\mathbf{1_{Co}}$ with the two cobalt(II) centers in a high-spin state (S = 3/2) with COSMO model (acetonitrile).

Table AI.4. The total energies (kcal/mol) of the cationic part of the compound **2** and compound **3** under gas phase and in acetonitrile with different spin states (S = 0 and 2).

2	S = 2	*S = 0*
Energy(gas)	-6476	-6500
Gibbs Energy(gas)	-6280	-6299
Energy(solvated)	-6608	-6638
Gibbs Energy(solvated)	-6412	-6437
3	S = 2	*S = 0*
Energy(gas)	-6052	-6069
Gibbs Energy(gas)	-5898	-5911
Energy(solvated)	-6070	-6097
Gibbs Energy(solvated)	-5916	-5939

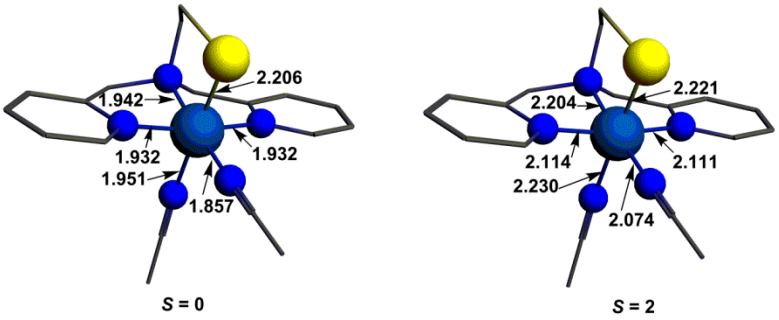

Figure AI.25. The optimized structures of the cationic part of compound **2** in different spin states with COSMO model (acetonitrile).

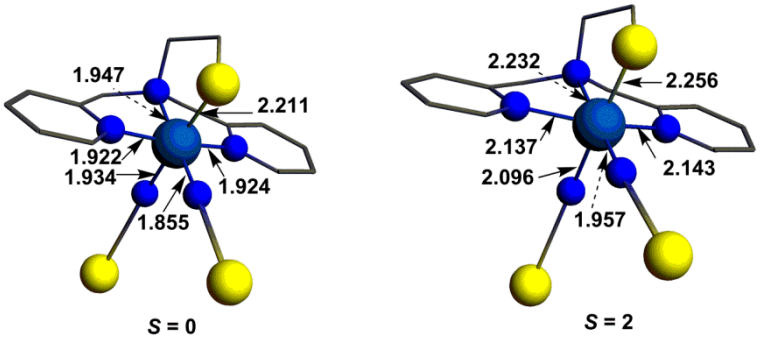

Figure AI.26. The optimized structure of compound **3** in different spin states with COSMO model (acetonitrile).

Table AI.5. The total energies (kcal/mol) of compound $\mathbf{1}_{Fe}$ under gas phase and solvent with different spin states.

($\mathbf{1}_{Fe}$)	***S* = 2, 2**	***S* = 0, 0**	***S* = 0, 2**
Energy(gas)	-10515.7	-10488.9	-10502.8
Gibbs Energy(gas)	-10214.5	-10178.9	-10197.5
Energy(solvated)	-10564.6	-10542.9	-10559.3
Gibbs Energy(solvated)	-10263.5	-10232.9	-10253.9

Table AI.6. The total energies (kcal/mol) of the compound $\mathbf{1_{Fe}}$ under gas phase and solvent with different spin states and keeping the Fe1-S1 bond frozen.

($\mathbf{1_{Fe}}$)	***S* = 2, 2**	***S* = 0, 0**	***S* = 0, 2**
Energy(gas)	-10513.6	-10476.9	-10497.2
Gibbs Energy(gas)	-10211.3	-10168.2	-10192.3
Energy(solvated)	-10564.8	-10528.0	-10544.7
Gibbs Energy(solvated)	-10262.6	-10219.3	-10239.8

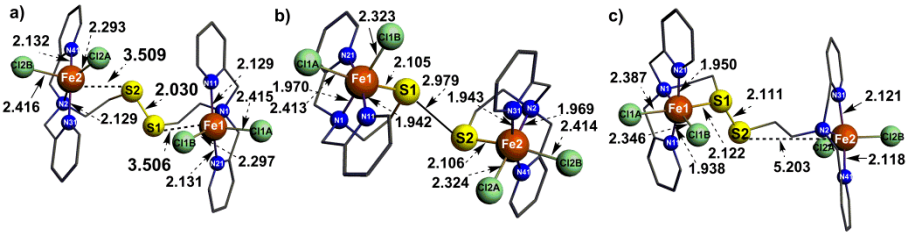

Figure AI.27. The optimized structures of the compound $\mathbf{1_{Fe}}$ with a) high-spin states (*S* = 2 for both iron center), b) low-spin states (*S* = 0 for both iron centers), c) mixed-spin states (*S* = 0 for one iron center, and *S* = 2 for another iron center) with COSMO model (methanol).

Table AI.7. The total energies (kcal/mol) of acetonitrile, and the cobalt compounds **5** and **6** with different spin states and their related antiferromagnetically coupled species (AF(1,1) is the antiferromagnetically coupled species obtained from the compound **5** with two triplet-spin cobalt(III) centers, AF(2,2) is the antiferromagnetically coupled species obtained from the compound **5** with two high-spin cobalt(III) centers).

5	S = 0, 0	S = 1,1	AF(1,1)	S =2,2	AF(2,2)
Energy (gas)	-9345	-9346	-9318	-9316	-9286
Gibbs energy (gas)	-9033	-9035	-9007	-9008	-8979
Energy (solvated)	-9816	-9812	-9788	-9772	-9742
Gibbs energy (solvated)	-9504	-9501	-9477	-9464	-9435
6	S = 0, 0		S =2,2		
Energy (gas)	-11089		The		
Gibbs energy (gas)	-10721		structure		
Energy (solvated)	-11535		has been		
Gibbs energy (solvated)	-11167		broken		

Table AI.8. The total energies (kcal/mol) of acetonitrile, and the copper compounds **7** and **8** (AF(1/2,1/2) is the antiferromagnetically coupled species obtained from the compound **8** with two doublet-spin copper(II) centers).

	Acetonitrile	**7**	**8**	AF(1/2,1/2)
Gibbs energy (gas)	-837	-5525	-9368	-9363
Energy (gas)	-850	-5696	-9676	-9671
Gibbs energy (solvated)	-844	-5569	-9487	-9483
Energy (solvated)	-857	-5740	-9795	-9791

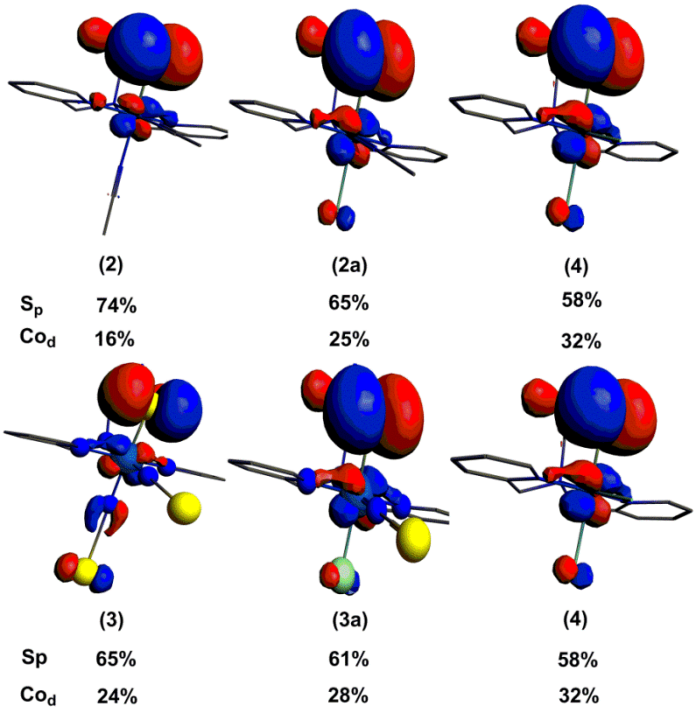

Figure AI.28. Plots showing the character of the HOMOs of compounds **2**, **3**, and the hypothetical compounds **2a**, **3a** and **4**.

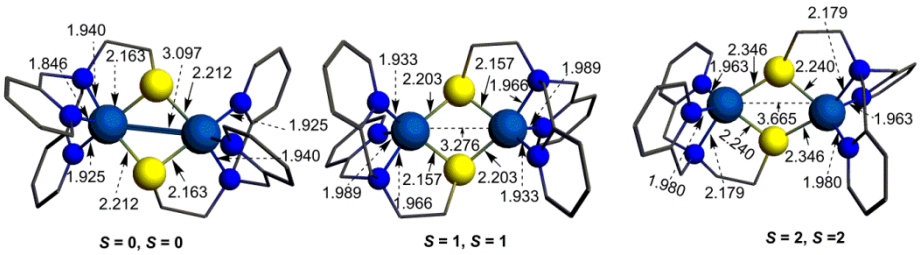

Figure AI.29. The optimized structures of compound **5** in different spin states with COSMO model (acetonitrile).

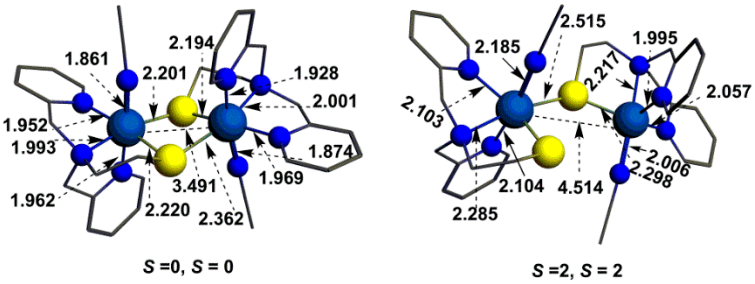

Figure AI.30. The optimized structures of compound **6** in different spin states with COSMO model (acetonitrile).

Appendix II

Supplementary information on Chapter 3

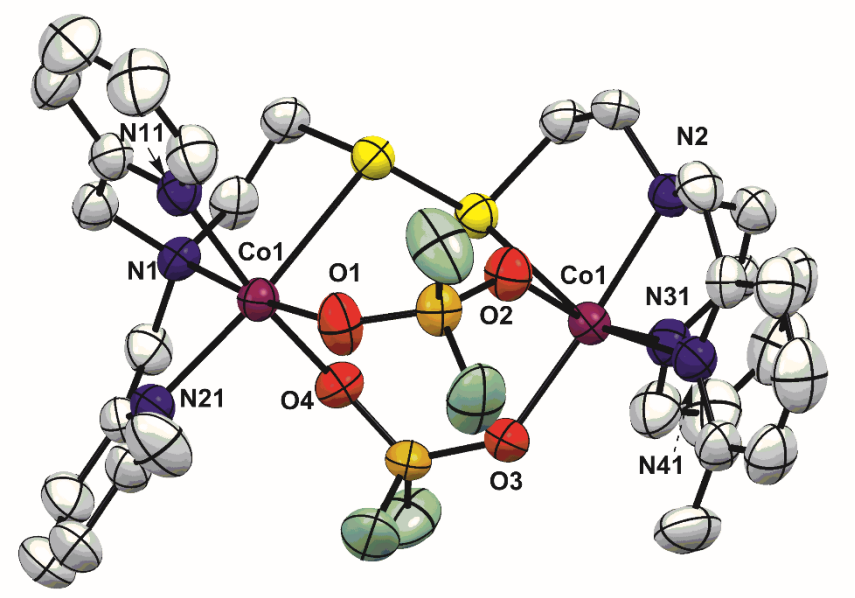

Figure AII.1. Displacement ellipsoid plot (50% probability level) of the compound $[Co^{II}_2(L^7SSL^7)(PO_2F_2)_2](PF_6)_2$ at 110(2) K. The lattice solvent molecule and hydrogen atoms are omitted for clarity.

Table AII.1. Experimental details for compounds $[Co^{II}_2(L^1SSL^1)(NO_3)_4]$ and $[Co^{II}_2(L^1SSL^1)(PO_2F_2)_2](PF_6)_2$.

Compounds	$[Co^{II}_2(L^1SSL^1)(NO_3)_4]$	$[Co^{II}_2(L^1SSL^1)(PO_2F_2)_2](PF_6)_2$
Chemical formula	$C_{28}H_{32}Co_2N_{10}O_{12}S_2$	$C_{28}H_{32}Co_2F_4N_6O_4P_2S_2 \cdot 2(F_6P) \cdot 3.338(CH_2Cl_2)$
M_r	882.61	1409.92
Crystal system, space group	Monoclinic, $P2_1/n$	Triclinic, P-1
Temperature (K)	110	110
a, b, c (Å)	8.1948 (2), 33.1859 (13), 13.6066 (8)	12.9871 (2), 13.7863 (3), 15.2272 (3)
β (°)	105.678 (3)	83.4006 (16)
V (Å^3)	3562.7 (3)	2616.93 (9)
Z	4	2
Radiation type	Mo $K\alpha$	Mo $K\alpha$
μ (mm^{-1})	1.12	1.28
Crystal size (mm)	0.18 × 0.12 × 0.06	0.37 × 0.26 × 0.16
Diffractometer	SuperNova, Dual, Cu at zero, Atlas	SuperNova, Dual, Cu at zero, Atlas
T_{min}, T_{max}	0.806, 1.000	0.473, 1.000
No. of measured, independent and observed [$I > 2\sigma(I)$] reflections	22306, 8369, 6063	40131, 11994, 10992
R_{int}	0.032	0.021
$(\sin\theta/\lambda)_{max}$ (Å^{-1})	0.623	0.650
$R[F^2 > 2\sigma(F^2)]$, $wR(F^2)$, S	0.040, 0.081, 0.90	0.030, 0.071, 1.04
No. of reflections	8369	11994
No. of parameters	501	844
No. of restraints	145	922
$\Delta\rho_{max}$, $\Delta\rho_{min}$ (e Å^{-3})	1.14, -0.77	1.22, -0.55

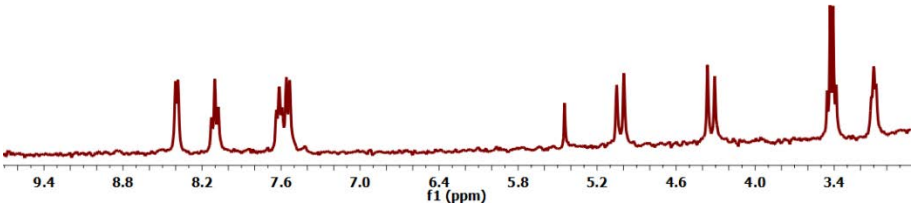

Figure AII.2. ^{1}H NMR spectrum of $[Co^{III}(L^{1}S)(MeCN)_2]^{2+}$, obtained upon dissolution of the compound $[Co^{II}_2(L^{1}SSL^{1})(PO_2F_2)_2](PF_6)_2$ in acetonitrile-d*3*.

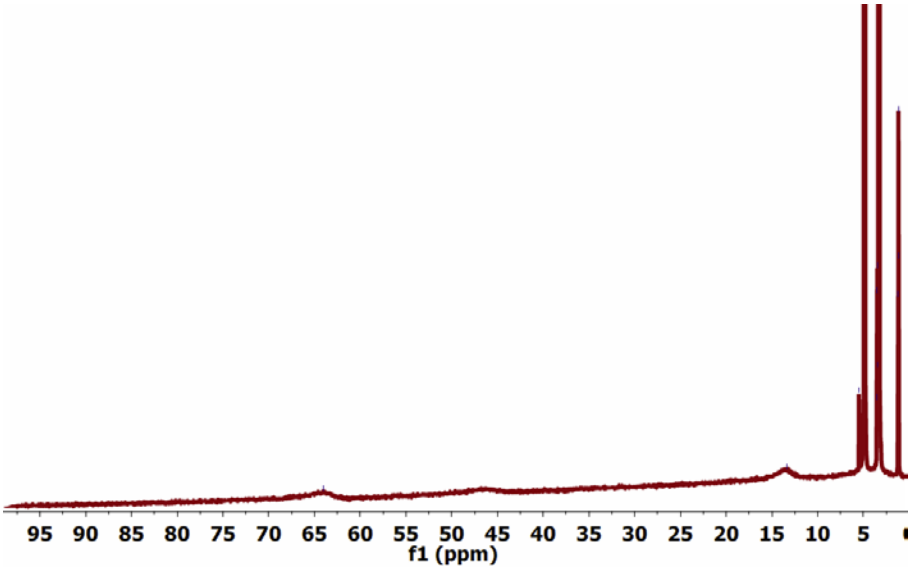

Figure AII.3. ^{1}H NMR spectrum of $[Co^{II}_2(L^{1}SSL^{1})(PO_2F_2)_2](PF_6)_2$ in methanol-d*4*.

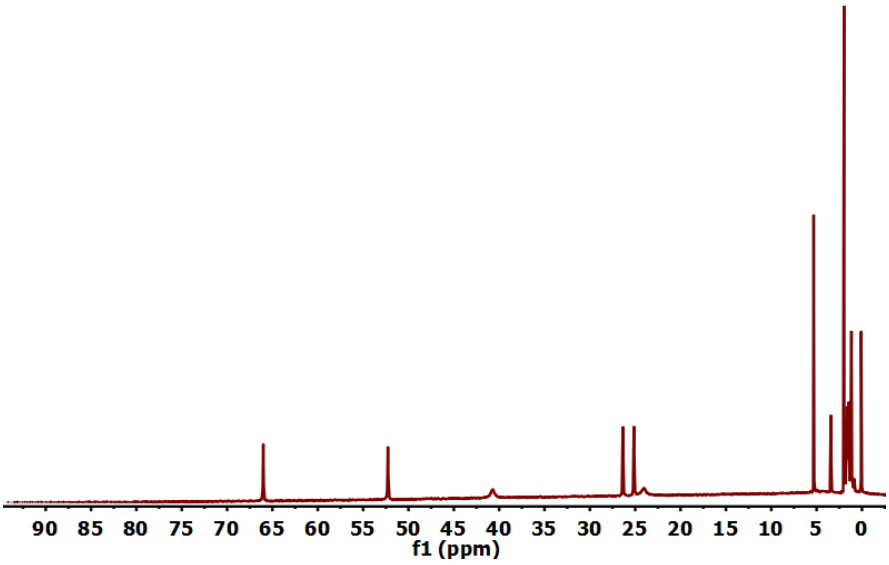

Figure AII.4. ^{1}H NMR spectrum of $[Co^{II}_2(L^1SSL^1)(PO_2F_2)_2](PF_6)_2$ in dichloromethane-d_2.

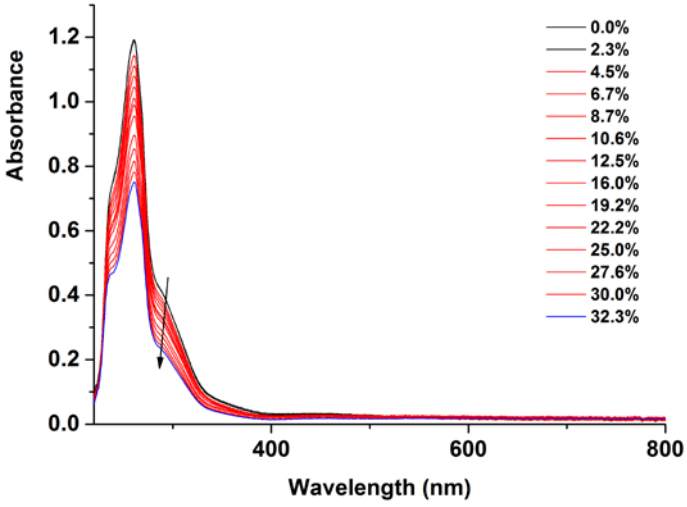

Figure AII 5. UV-vis spectra of $[Co^{II}_2(L^1SSL^1)(PO_2F_2)_2](PF_6)_2$ dissolved in 4.2 mL acetonitrile with variable amounts of dichloromethane added at 1.1 mM [Co] concentration recorded with a transmission dip probe at a path length of 1.8 mm.

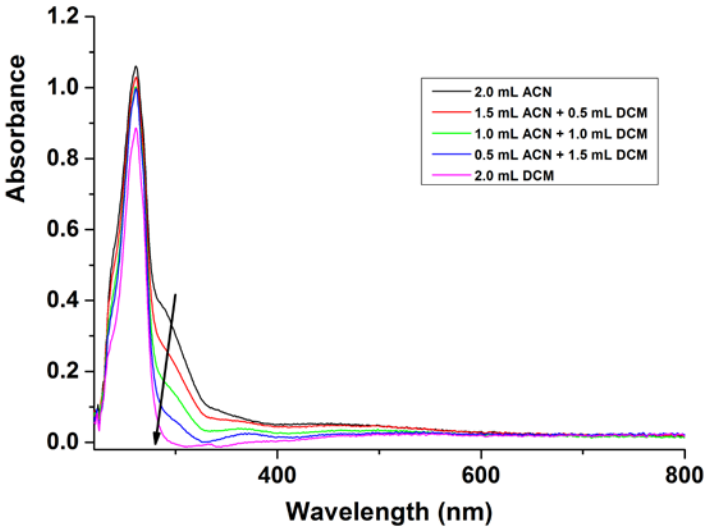

Figure AII 6. UV-vis spectra of the different ratios of acetonitrile and dichloromethane solution of $[Co^{II}_2(L^1SSL^1)(PO_2F_2)_2](PF_6)_2$ in 10 mL at 1.1 mM [Co] concentration recorded with a transmission dip probe at a path length of 1.8 mm.

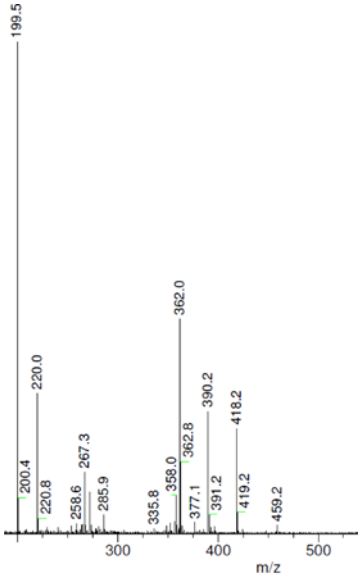

Figure AII.7. ESI-MS spectrum of $[Co^{II}_2(L^1SSL^1)(PO_2F_2)_2](PF_6)_2$ dissolved in acetonitrile. ESI-MS combined with simulated spectrum found (calcd) for ½$[Co(L^1S) + 2MeCN]^{2+}$ *m/z* 199.5 (195.5); $[Co(L^1S) + PO_2F_2]^+$ m/z 418.2 (418.1); $[Co(L^1S) + PO_2F_2 + MeCN]^+$ 459.2 (459.1).

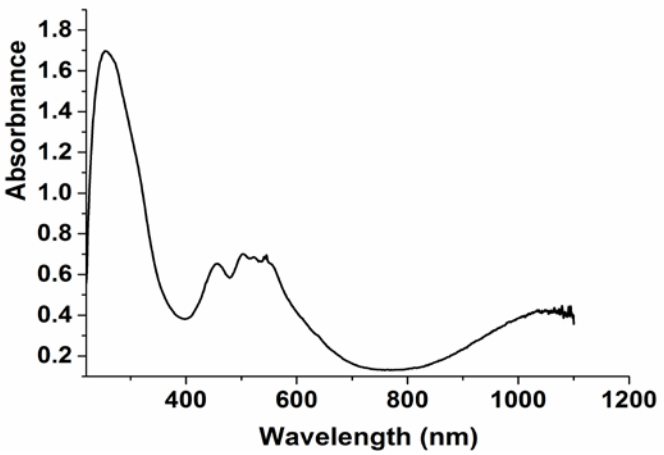

Figure AII.8. UV-vis spectrum for the solid sample of $[Co^{II}_2(L^1SSL^1)(PO_2F_2)_2](PF_6)_2$ obtained from a dichloromethane solution.

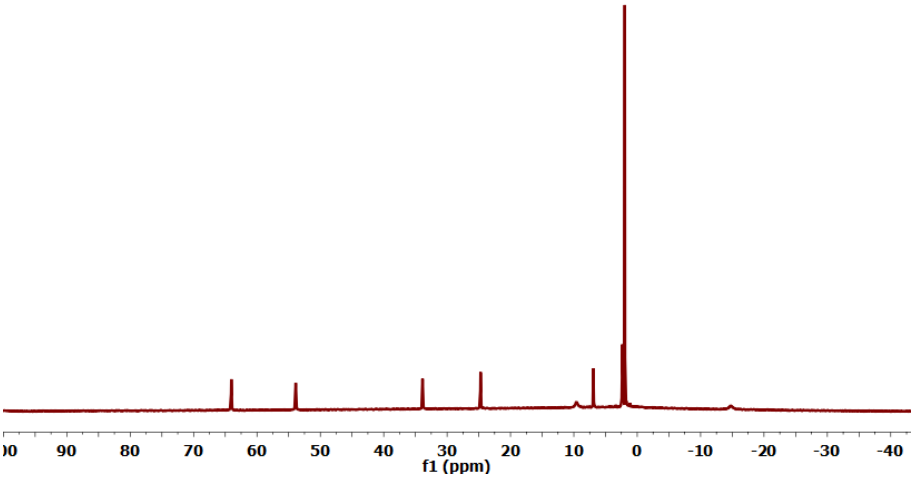

Figure AII.9. ^1H NMR spectrum of the compound $[Co^{II}_2(L^7SSL^7)(PO_2F_2)_2](PF_6)_2$ in acetonitrile-d_3.

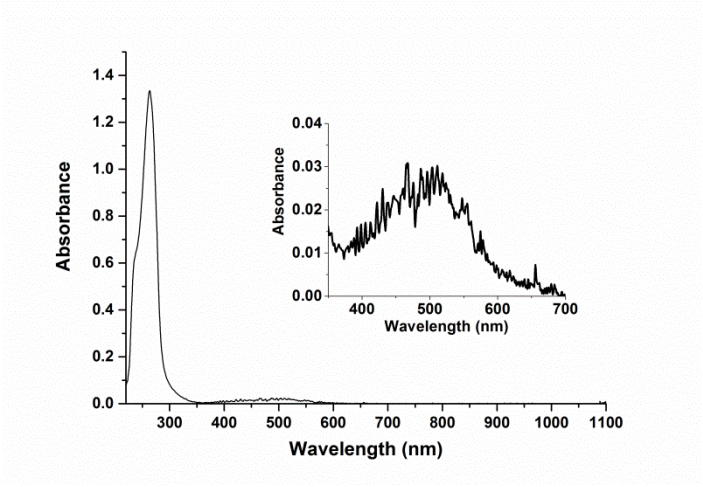

Figure AII.10. UV-vis spectrum of the compound $[Co^{II}_2(L^7SSL^7)(PO_2F_2)_2](PF_6)_2$ in acetonitrile. UV-vis spectra in solution were recorded using a solution 2 mM in [Co] with a transmission dip probe path length of 1.2 mm. The inset shows the solution 4 mM in [Co].

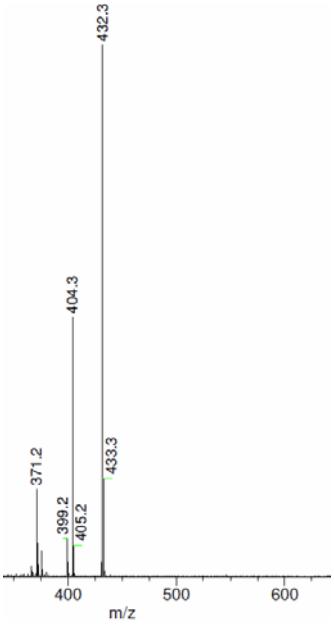

Figure AII.11. ESI-MS spectrum of $[Co^{II}_2(L^7SSL^7)(PO_2F_2)_2](PF_6)_2$ dissolved in acetonitrile. ESI-MS found (calcd) for $[Co^{II}_2(L^7SSL^7)(PO_2F_2)_2]^{2+}$ *m/z* 432.3 (432.1).

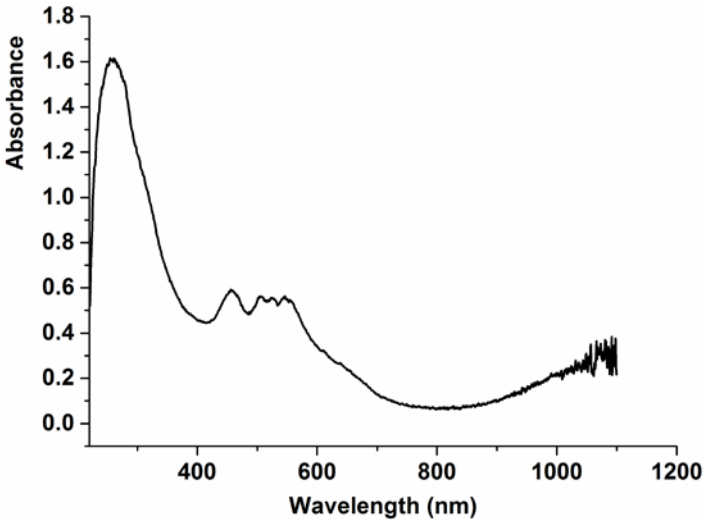

Figure AII.12. UV-vis spectrum for the solid sample of $[Co^{II}_2(L^7SSL^7)(PO_2F_2)_2](PF_6)_2$.

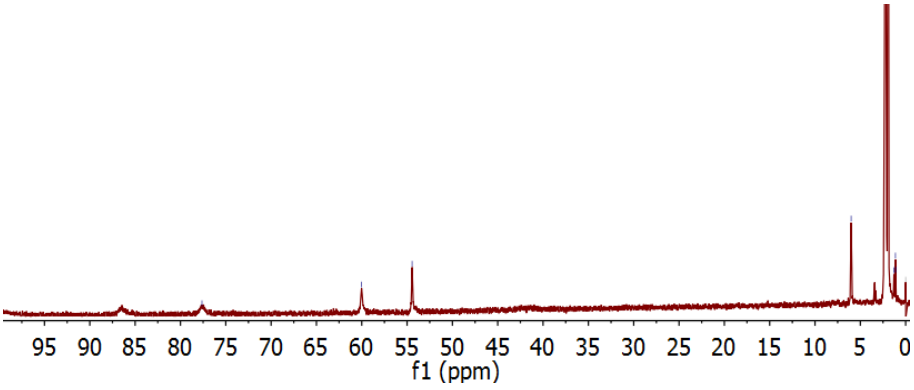

Figure AII.13. ^1H NMR spectrum of compound $[Co^{II}_2(L^1SSL^1)(NO_3)_4]$ dissolved in acetonitrile-d_3.

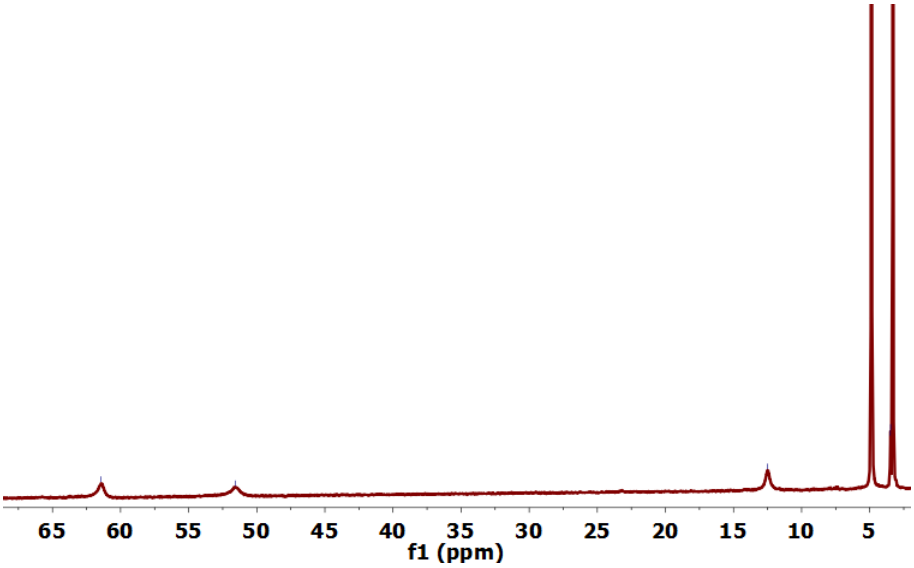

Figure AII.14. ^{1}H NMR spectrum of compound $[Co^{II}_2(L^{1}SSL^{1})(NO_3)_4]$ dissolved in methanol-d_4.

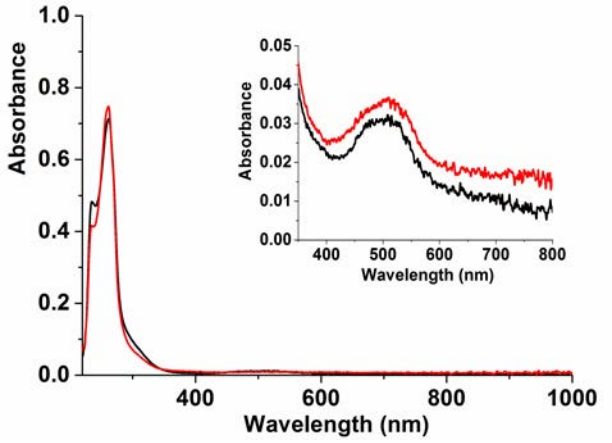

Figure AII.15. UV-vis spectra of the compound $[Co^{II}_2(L^{1}SSL^{1})(NO_3)_4]$ in methanol (red line) and in acetonitrile (black line). UV-vis spectra were recorded using solutions 1 mM in [Co] with a transmission dip probe path length of 1.4 mm. The inset shows the UV-vis spectra of 2 mM [Co] in acetonitrile (black) with a path length of 1.4 mm and 2 mM [Co] in methanol (red) with a path length of 1.8 mm.

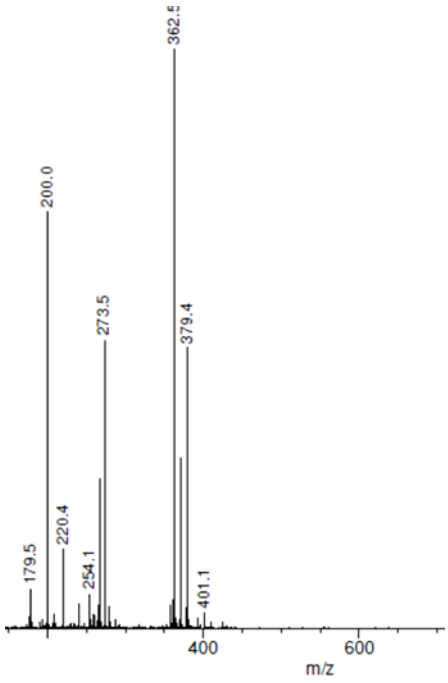

Figure AII.16. ESI-MS spectrum of the compound $[Co^{II}_2(L^1SSL^1)(NO_3)_4]$ in acetonitrile, ESI-MS found (calcd) for ½ $[M - 2\ NO_3]^{2+}$ *m/z* 379.4 (379.3); ½ $[M - 4\ NO_3 + 2HCO_2]^{2+}$ *m/z* 362.5 (362.1).

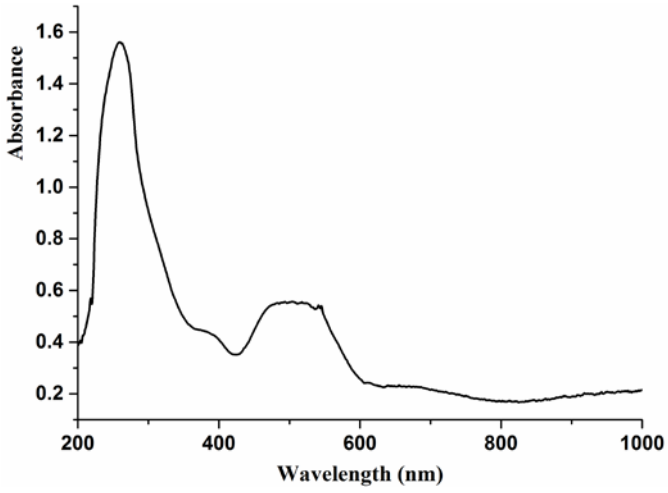

Figure AII.17. UV-vis spectrum of the compound $[Co^{II}_2(L^1SSL^1)(NO_3)_4]$ in the solid state.

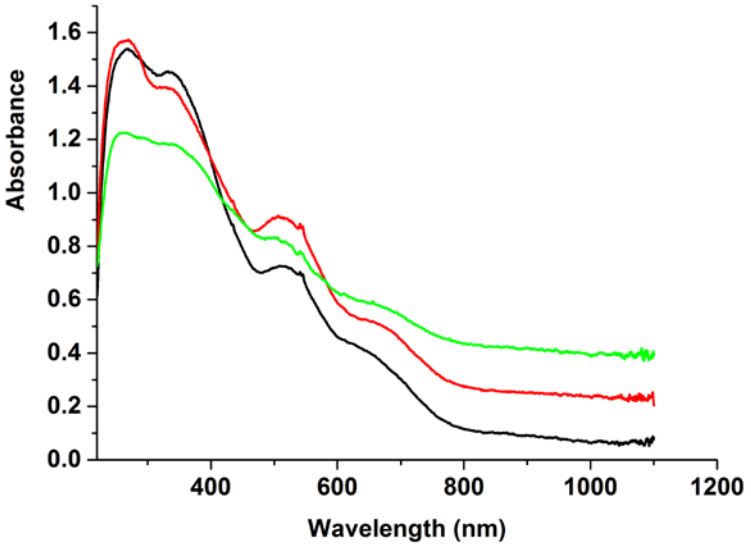

Figure AII.18. UV-vis spectra of the compound $[Co^{III}(L^1S)(NCS)_2]$ in the solid state obtained from acetonitrile (black line), methanol (red line), and acetone (green line).

Appendix III

Supplementary information on Chapter 4

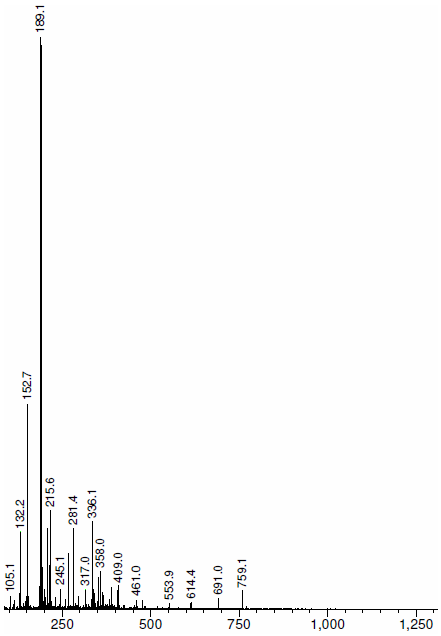

Figure AIII.1. ESI-MS spectrum of the Fe(III) compound **2** dissolved in methanol. ESI-MS found (calcd) for ½[Fe(L^1SO_3)(H_2O)]$^{2+}$ *m/z* 189.2 (190.0).

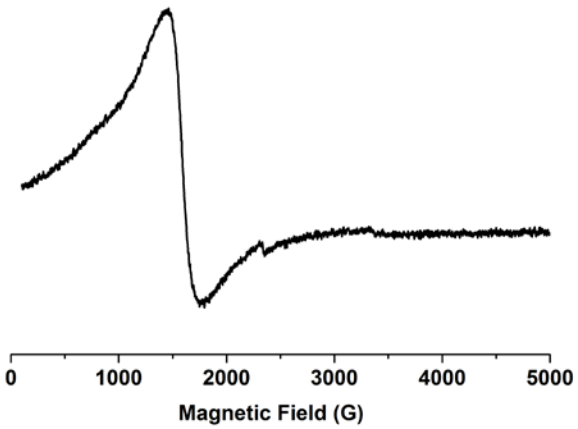

Figure AIII.2. EPR spectrum of the compound **2** dissolved in DMSO. The experiment was performed at 20 K.

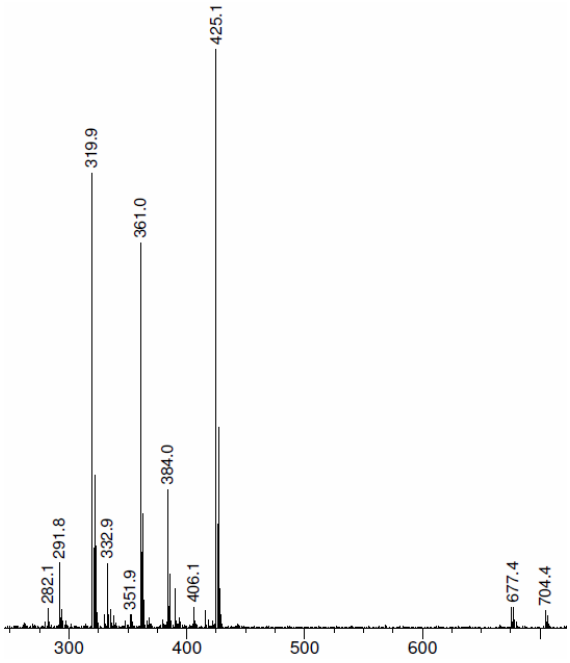

Figure AIII.3. ESI-MS spectrum of the Co(III) compound **4** dissolved in acetonitrile. ESI-MS found (calcd) for $[Co^{III}(L^1SO_2)Cl]^+$ *m/z* 384.4 (384.0); $[Co^{III}(L^1SO_2)Cl + MeCN]^+$ *m/z* 425.5 (425.1).

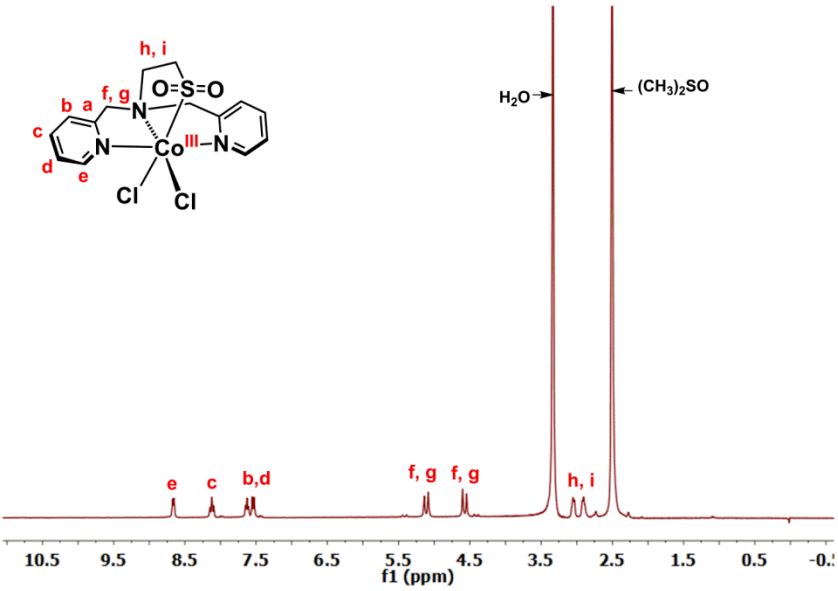

Figure AIII.4. NMR spectrum of compound **4** dissolved in DMSO-d_6.

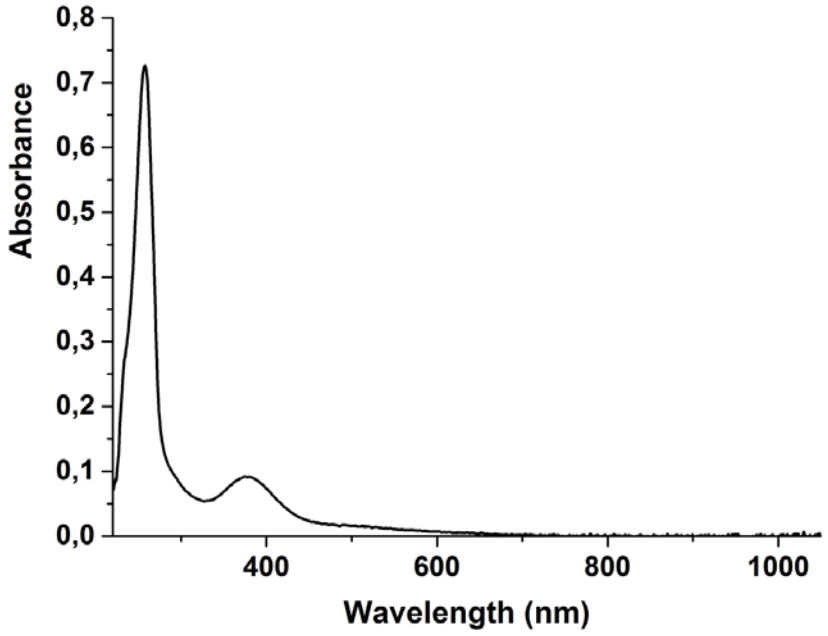

Figure AIII.5. UV-vis spectrum of compound **2** dissolved in methanol. UV-Vis spectra in solution were recorded using a solution 1 mM in [Fe] with a transmission dip probe path length of 1.8 mm.

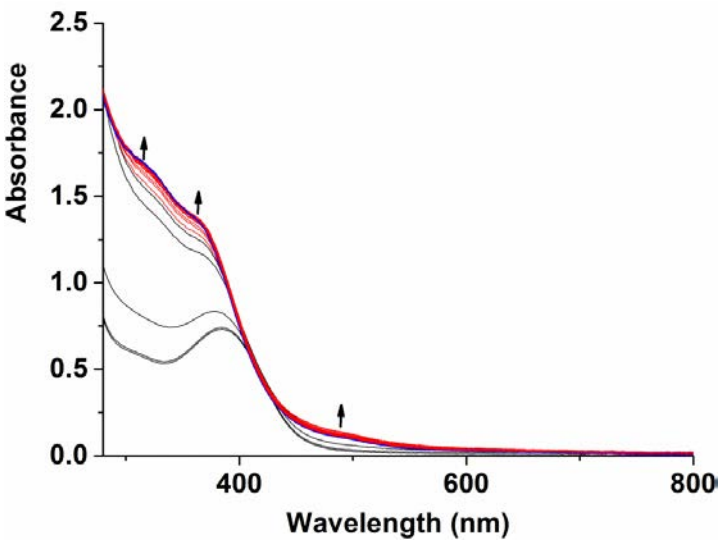

Figure AIII.6. The change of UV–vis spectra upon addition of H_2O_2 (0.2 mmol, 40 equivalents to the compound **1**) to compound **1** in methanolic solution in the first two minutes under room temperature. UV-vis spectra were recorded using a solution 2 mM in [Fe] (5 mL) with a transmission dip probe path length of 2.8 mm. Spectra recorded every 1 second over a period of 5 minutes.

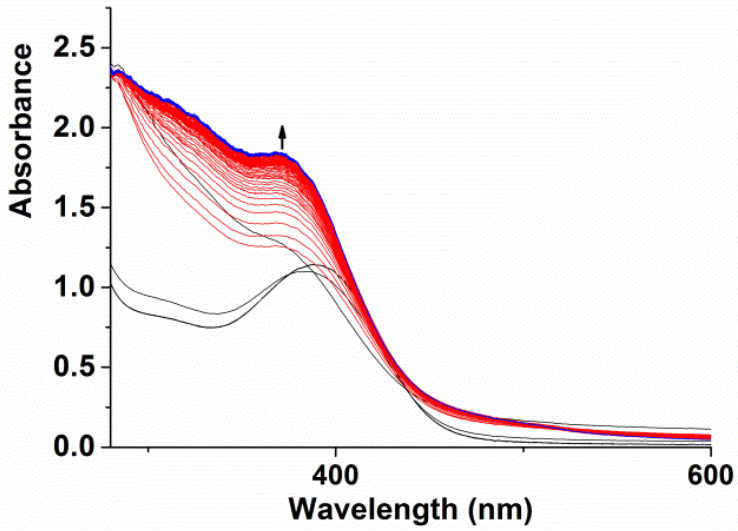

Figure AIII.7. The change of UV–vis spectra upon addition of H_2O_2 (0.8 mmol, 80 equivalents to the compound **1**) to compound **1** in methanolic solution in the first two minutes under room temperature. UV-vis spectra were recorded using a solution 4 mM in [Fe] (5 mL) with a transmission dip probe path length of 2.8 mm. Spectra recorded every 1 second over a period of 3 minutes.

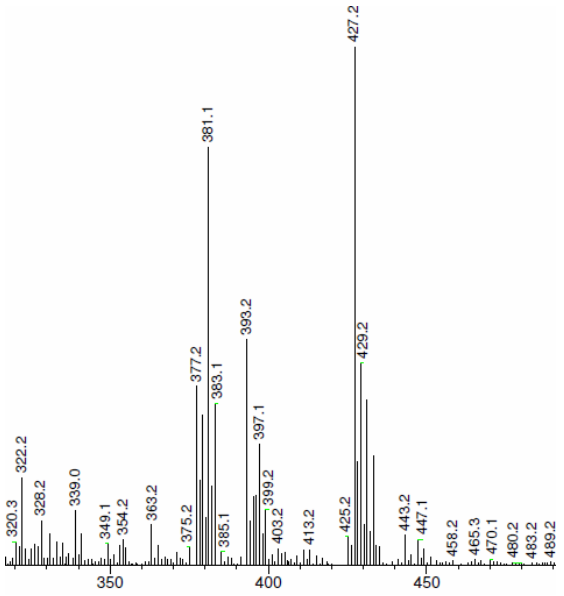

Figure AIII.8. ESI-MS spectrum of reaction mixture of the compound **1** with excess 35% H_2O_2 (80 equivalents to the compound **1**) in methanol at −78 °C. ESI-MS found (calcd) for $[Fe^{III}(L^1SO_2)Cl]^+$ *m/z* 381.1 (381.0); $[Fe^{III}(L^1SO_3)Cl]^+$ *m/z* 397.1 (397.0), $[Fe^{III}(L^1SO_3)Cl + CH_3OH]^+$ *m/z* 429.2 (429.1).

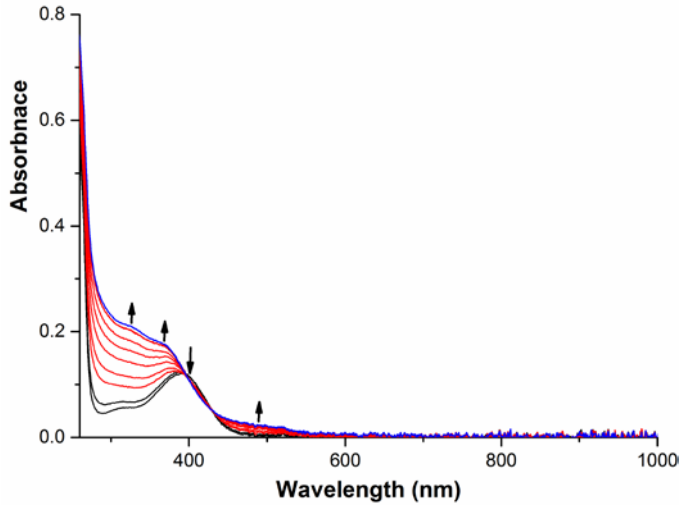

Figure AIII.9. The change in UV-vis when H_2O_2 (5 μL/each time) was titrated into a solution of compound **1** in methanol at room temperature. UV-vis spectra were recorded using a solution 2 mM in [Fe] (10 mL) with a transmission dip probe path length of 0.9 mm.

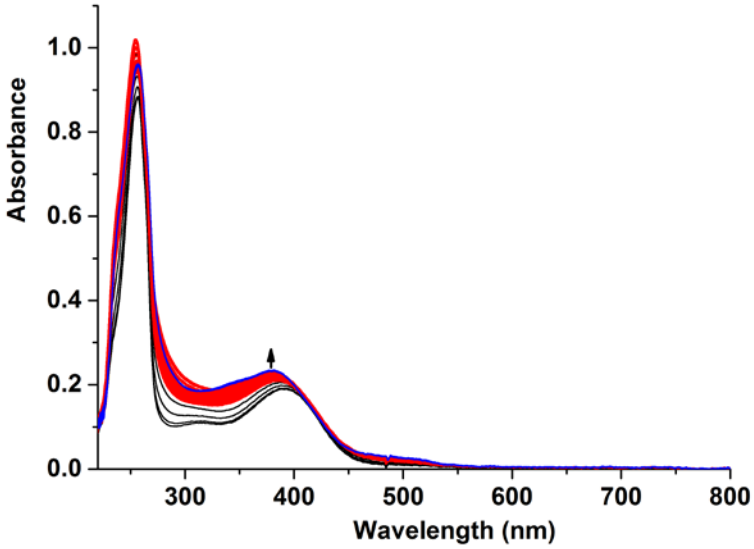

Figure AIII.10. The change of UV-vis spectral when ^{t}BuOOH (0.2 mmol, 40 equivalents to the compound **1**) was added to compound **1** dissolved in methanol. UV-vis specctra were recorded using a solution 2 mM in [Fe] (5 mL) with a transmission dip probe path length of 0.9 mm at –41 ^{o}C. Spectra recorded every 30 seconds over a period of 3 minutes, and then recorded every 3 seconds over a period of 20 minutes.

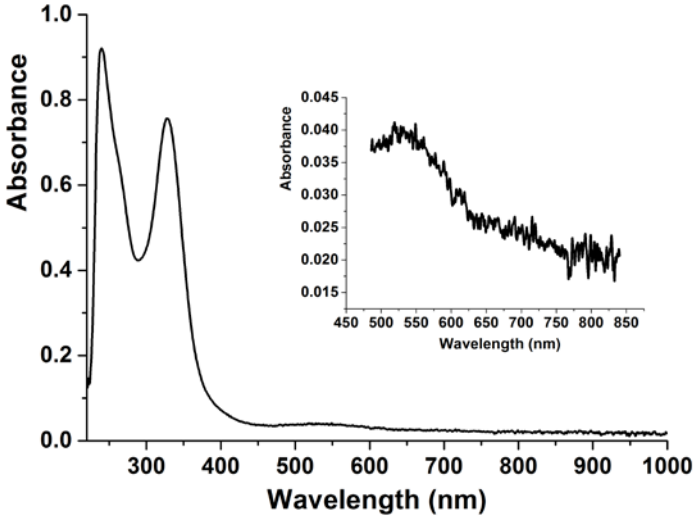

Figure AIII.11. UV-vis spectrum of compound **4** dissolved in acetonitrile. The UV-vis spectrum was recorded using the solution 1 mM in [Co] with a transmission dip probe path length of 1.6 mm at room temperature. The inset shows the amplified part of UV-vis spectra from 450 nm to 850 nm.

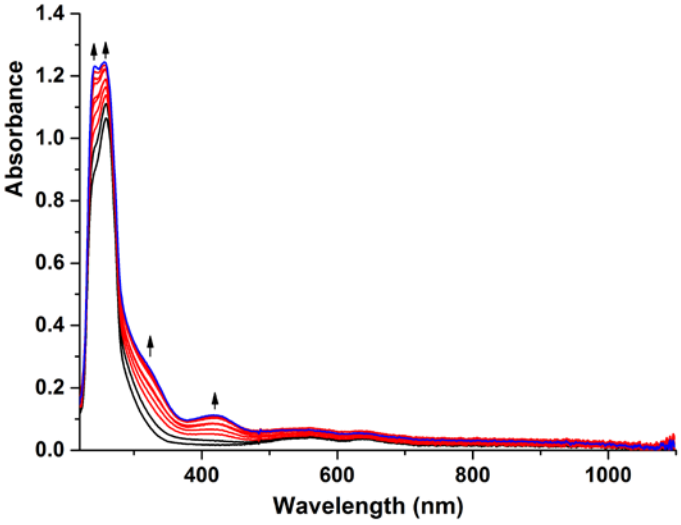

Figure AIII.12. The change in UV-vis spectra when H_2O_2 (5 μL/each time) was titrated into a solution of compound **3** in acetonitrile at room temperature. UV-vis specctra were recorded using a solution 2 mM in [Co] (10 mL) with a transmission dip probe path length of 1.3 mm.

Figure AIII.13. ESI-MS spectrum of the reaction mixture of **3** with H_2O_2 after the first one hour. ESI-MS found (calcd) for $[Co^{III}(L^1SO)Cl]^+$ *m/z* 368.1 (368.0); $[Co^{III}(L^1SO_2)Cl$ + MeCN$]^+$ *m/z* 425.1 (425.0).

Table AIII.1. Crystallographic and structures refinement data for compounds **2** and **4**.

	2	**4**
Chemical formula	$2(C_{14}H_{16}Cl_2FeN_3O_3S)\cdot C_3H_7NO$	$C_{14}H_{16}Cl_2CoN_3O_2S\cdot 3(H_2O)$
Formula Weight	939.31	474.23
Crystal System	monoclinic	monoclinic
Space Group	$P2_1/c$	$P2_1/n$
a (Å)	14.059(4)	8.3845(3)
b (Å)	22.0371(6)	14.5303(4)
c (Å)	12.5600 (3)	15.1848(5)
α (°)	90	90
β (°)	100.192(2)	91.740(3)
γ (°)	90	90
V (Å^3)	3829.96(18)	1849.10(10)
Z	4	4
D_{calc} (g.cm^3)	1.629	1.703
$T_{min}-T_{max}$	0.449, 1.000	0.642,1.000
Crystal Size(mm)	0.60 x 0.28 x 0.10	0.36 x 0.21 0.12
μ (mm^{-1})	1.201	1.362
No. of Reflections	35704	14470
No. of unique reflections	8788	4242
No. of reflections observed [I > 2σ(I)]	7513	3698
No. of parameters	480	260
R1/WR2 [I > 2σ(I)]	0.0301, 0.0650	0.0288,0.0699
R1/WR2 [all reflections]	0.0390, 0.0696	0.0346, 0.0736
Goodness of fit (GOF)	1.063	1.045
Residual electron density (e Å^{-3})	0.49/-0.40	0.49/-0.37

Appendix IV

Supplementary information on Chapter 5

Table AIV.1. Crystallographic and structure refinement data for complex $[Fe^{II}_4(L^1SSL^1)_2F_6(MeCN)_2](BF_4)_2$.

$[Fe^{II}_4(L^1SSL^1)_2F_6(MeCN)_2](BF_4)_2$	
chemical formula	$C_{60}H_{70}F_6Fe_4N_{14}S_4{\cdot}4(BF_4)$
M_r	1800.18
crystal system, space group	Monoclinic, $C2/c$
Temperature (K)	110
a, b, c (Å)	15.0882(6), 19.6485(8), 25.1426(9)
β (°)	101.306(4)
V (Å^3)	7309.1(5)
Z	4
Radiation type	Mo $K\alpha$
μ (mm^{-1})	1.00
Crystal size (mm)	0.21 × 0.20 × 0.08
Diffractometer	SuperNova, Dual, Cu at zero, Atlas diffractometer
T_{min}, T_{max}	0.852, 0.944
No. of measured, independent and observed [$I > 2\sigma(I)$] reflections	28835, 8397, 6664
R_{int}	0.034
$(\sin\theta/\lambda)_{max}$ (Å^{-1})	0.650
$R[F^2 > 2\sigma(F^2)]$, $wR(F^2)$, S	0.042, 0.107, 1.04
No. of reflections	8397
No. of parameters	909
No. of restraints	1943
	$w = 1/[\sigma^2(F_o^2) + (0.0439P)^2 + 14.6984P]$ where $P = (F_o^2 + 2F_c^2)/3$
$\Delta\rho_{max}$, $\Delta\rho_{min}$ (e Å^{-3})	0.77, -0.53

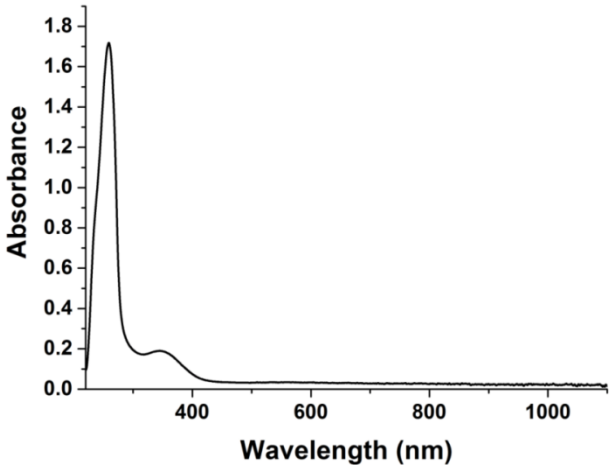

Figure AIV.1. UV-vis spectrum of the complex $[Fe^{II}_4(L^1SSL^1)_2F_6(MeCN)_2](BF_4)_2$ in acetonitrile at room temperature. 1 mM [Fe] with a transmission dip probe path length of 0.31 cm.

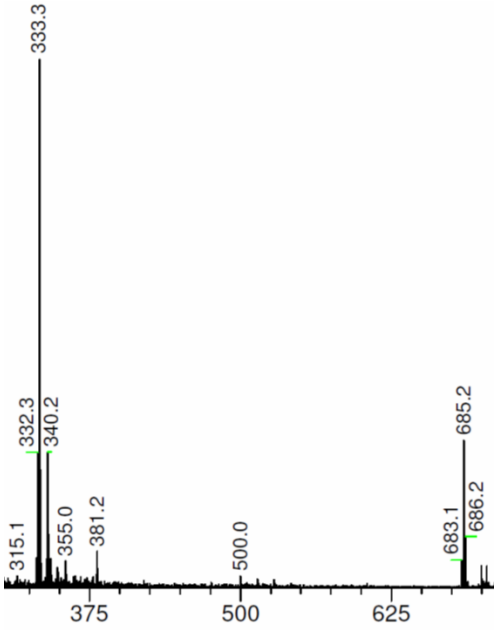

Figure AIV.2. ESI-MS spectrum of compound $[Fe^{II}_4(L^1SSL^1)_2F_6(MeCN)_2](BF_4)_2$ in acetonitrile.

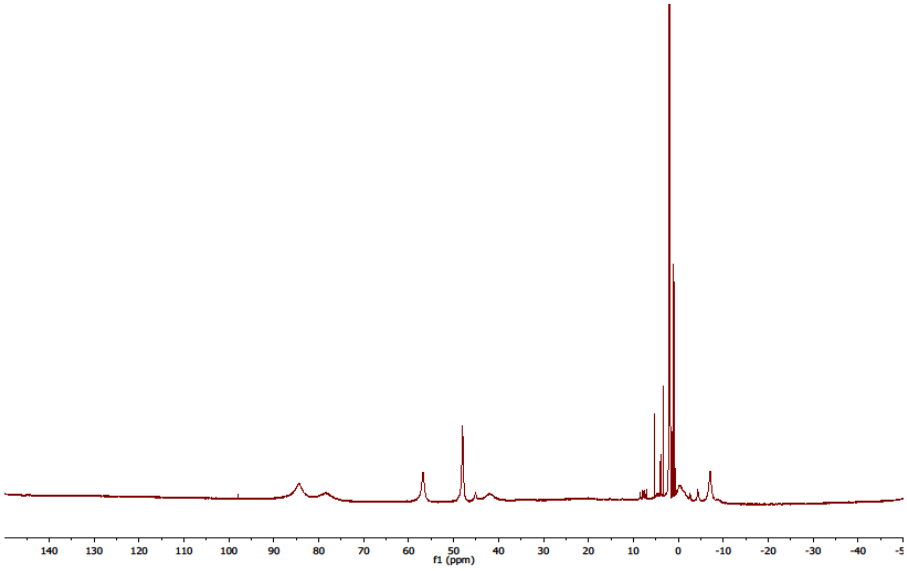

Figure AIV.3. ^{1}H NMR spectrum of the complex $[Fe^{II}_4(L^1SSL^1)_2F_6(MeCN)_2](BF_4)_2$ in acetonitrile-d_3 at room temperature.

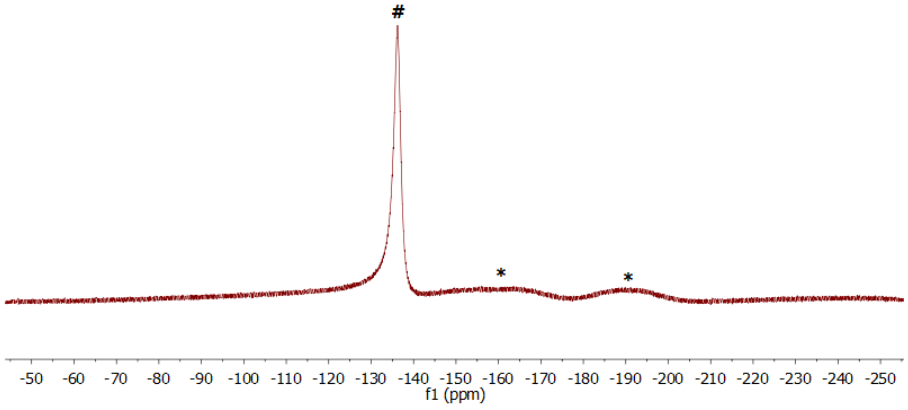

Figure AIV.4. ^{19}F NMR spectrum of complex $[Fe^{II}_4(L^1SSL^1)_2F_6(MeCN)_2](BF_4)_2$ in acetonitrile-d_3 at room temperature.

Appendix V

Supplementary information on Chapter 6

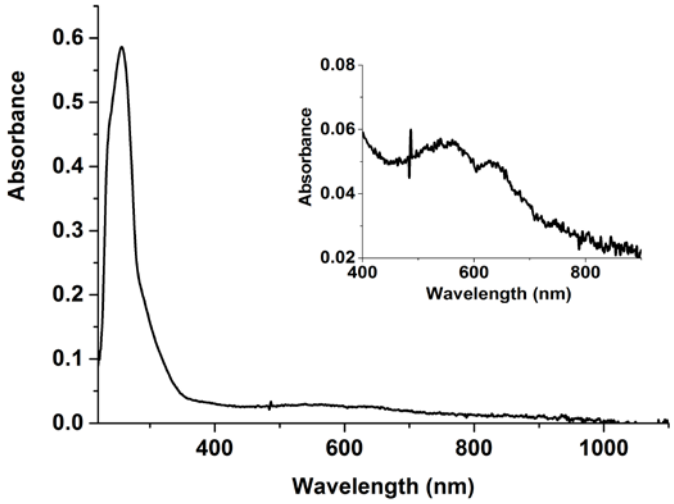

Figure AV.1. UV-vis spectrum of the compound $[Co^{II}(L^1SCH_3)Cl_2]$ dissolved in acetonitrile, recorded using solution 1 mM in [Co] with a transmission dip probe path length of 1.3 mm. The inset shows the UV-vis spectrum recorded of a solution 2 mM in [Co].

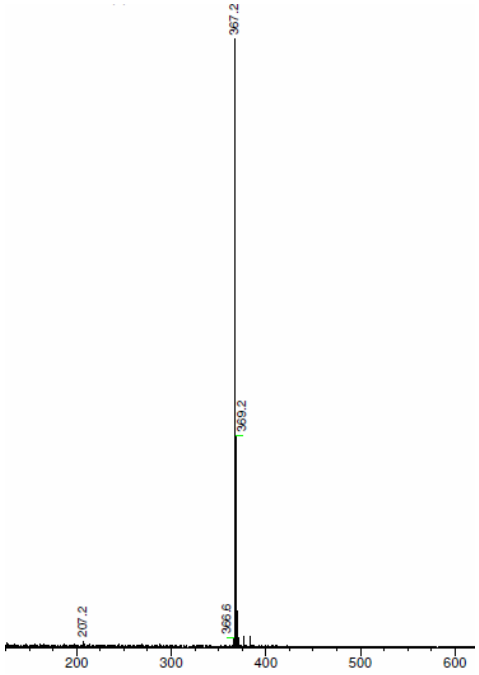

Figure AV.2. ESI-MS spectrum of the compound $[Co^{II}(L^{1}SCH_3)Cl_2]$ dissolved in acetonitrile. ESI-MS found (calcd) for $[M-Cl]^+$ *m/z* 367.2 (367.1).

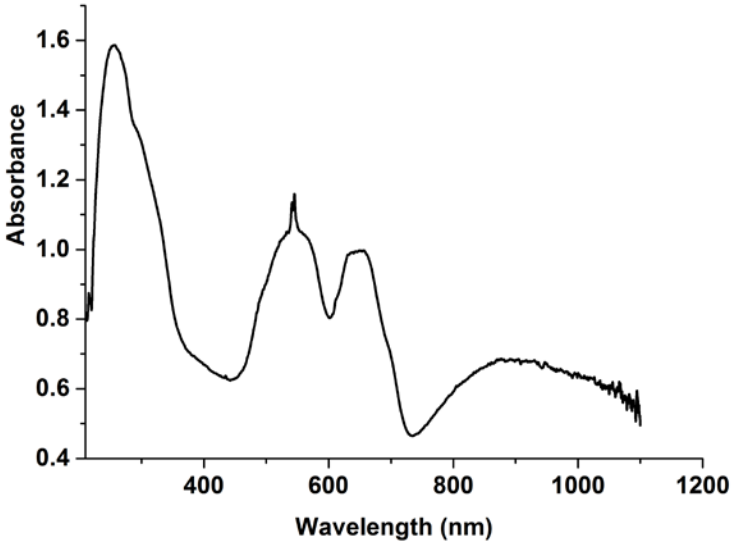

Figure AV.3. UV-vis spectrum of the compound $[Co^{II}(L^{1}SCH_3)Cl_2]$ in the solid state.

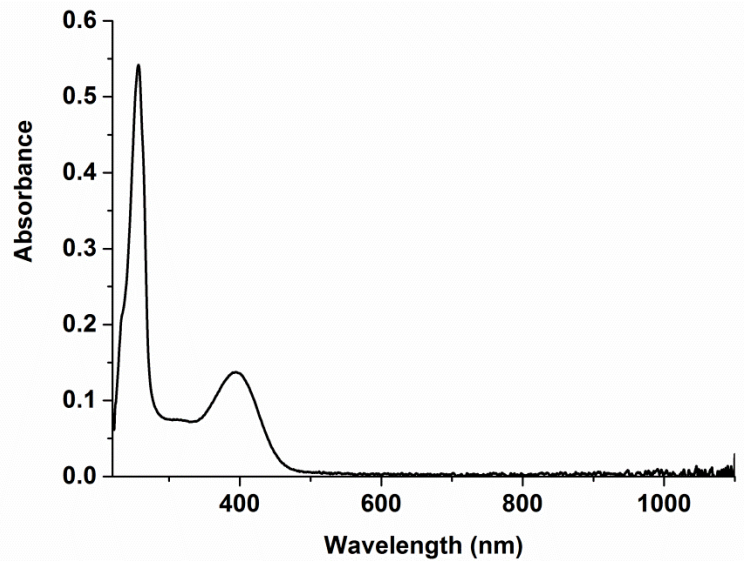

Figure AV.4. UV-vis spectrum of the compound $[Fe^{II}(L^1SCH_3)Cl_2]$ dissolved in methanol, recorded using a solution 1 mM in [Fe] with a transmission dip probe path length of 1.3 mm.

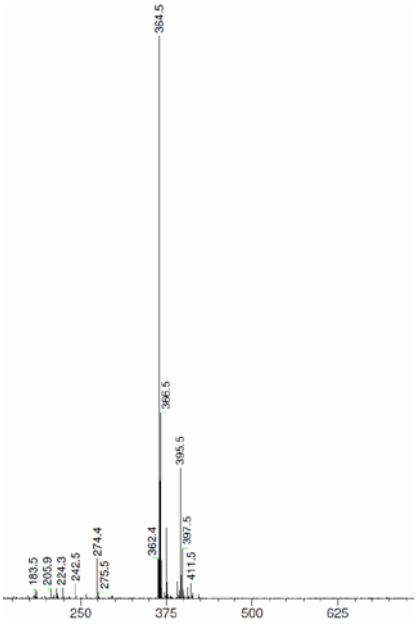

Figure AV.5. ESI-MS spectrum of the compound $[Fe^{II}(L^1SCH_3)Cl_2]$ dissolved in methanol. ESI-MS found (calcd) for $[M-Cl]^+$ *m/z* 364.5 (364.1).

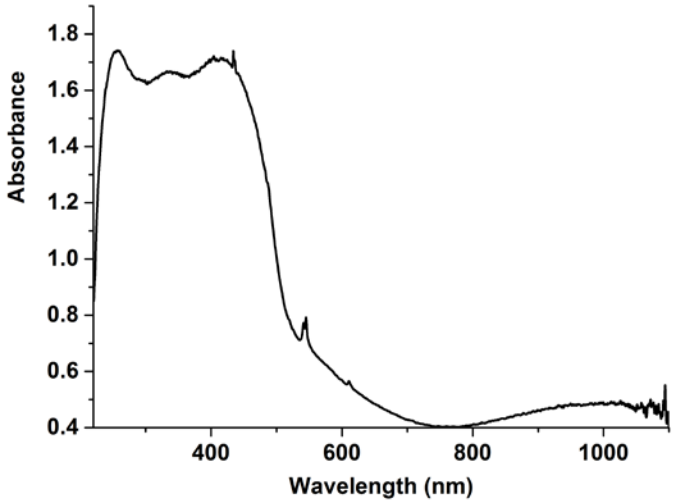

Figure AV.6. UV-vis spectrum of the compound $[Fe^{II}(L^1SCH_3)Cl_2]$ in the solid state.

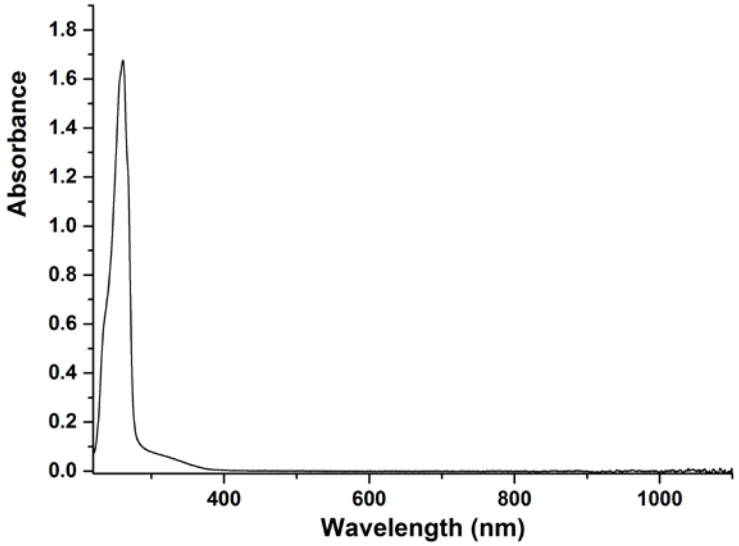

Figure AV.7. UV-vis spectrum of the compound $[Mn^{II}(L^1SCH_3)Cl_2]$ dissolved in acetonitrile, recorded using a solution 1 mM in [Mn] with a transmission dip probe path length of 1.2 mm.

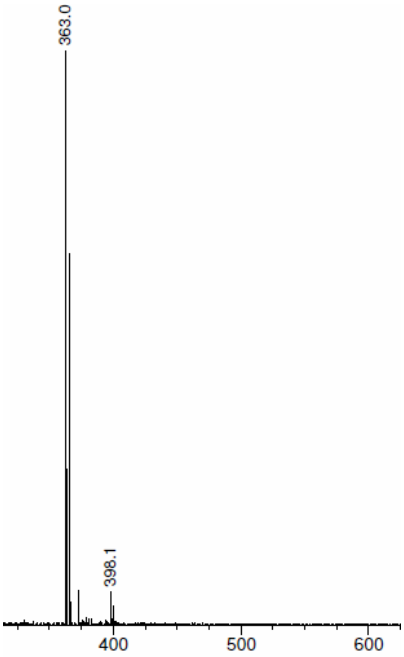

Figure AV.8. ESI-MS spectrum of the compound $[Mn^{II}(L^1SCH_3)Cl_2]$ in the methanol. ESI-MS found (calcd) for $[M-Cl]^+$ *m/z* 363.0 (363.1).

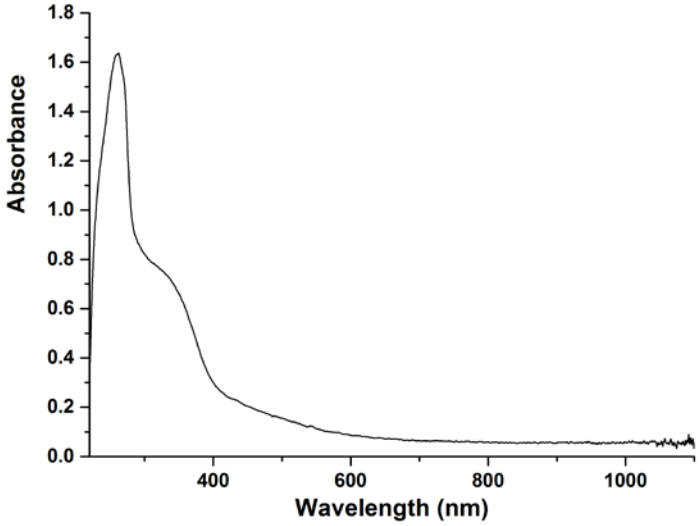

Figure AV.9. UV-vis spectrum of the compound $[Mn^{II}(L^1SCH_3)Cl_2]$ in the solid state.

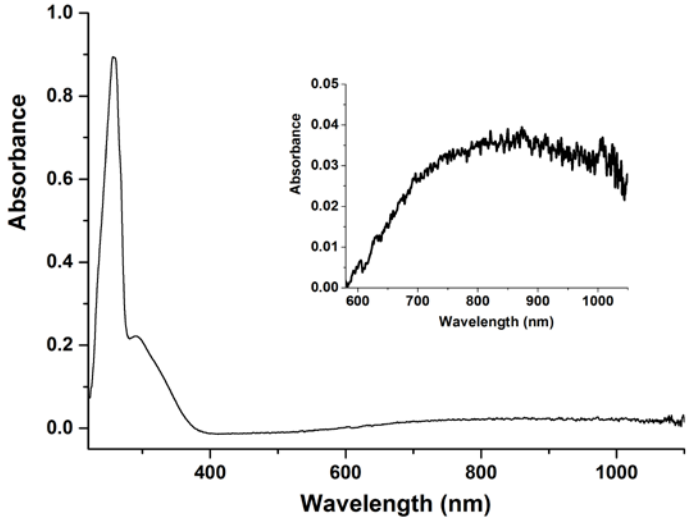

Figure AV.10. UV-vis spectrum of the compound $[Cu^{II}(L^1SCH_3)Cl_2]$ dissolved in acetonitrile, recorded using a solution 1 mM in [Cu] with a transmission dip probe path length of 1.2 mm. The inset shows the UV-vis spectrum of a solution 2 mM in [Cu].

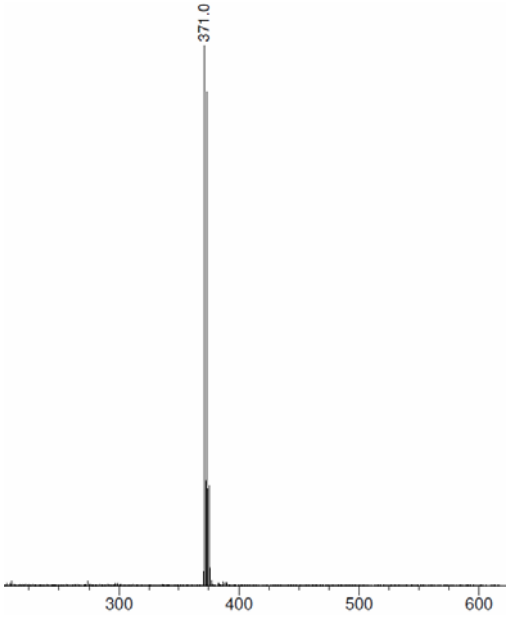

Figure AV.11. ESI-MS spectrum of the compound $[Cu^{II}(L^1SCH_3)Cl_2]$ in the methanol. ESI-MS found (calcd) for $[M-Cl]^+$ *m/z* 371.0 (371.0).

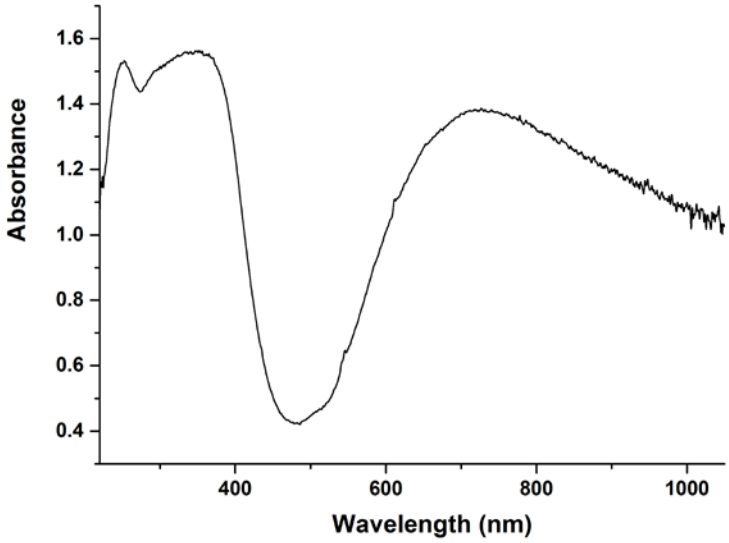

Figure AV.12. UV-vis spectrum of the compound $[Cu^{II}(L^1SCH_3)Cl_2]$ in the solid state.

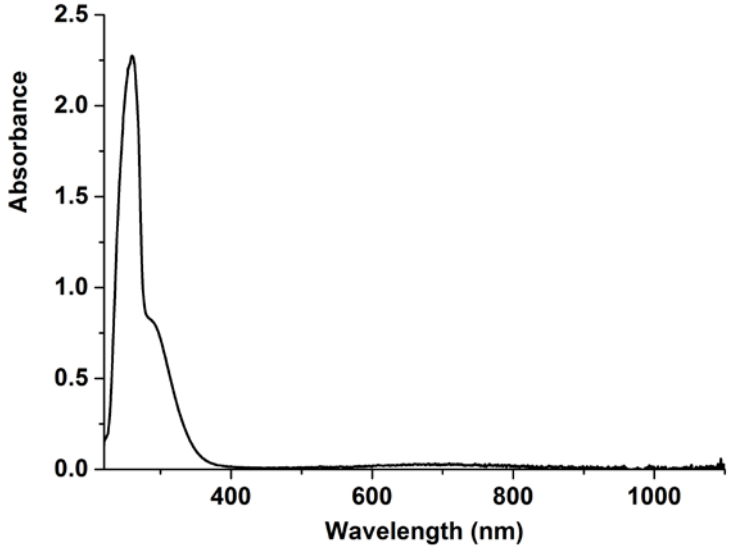

Figure AV.13. UV-vis spectrum of the compound $[Cu^{II}_2(L^1SSL^1)Cl_4]$ dissolved in methanol, recorded using a solution 5 mM in [Cu] with a transmission dip probe path length of 0.9 mm.

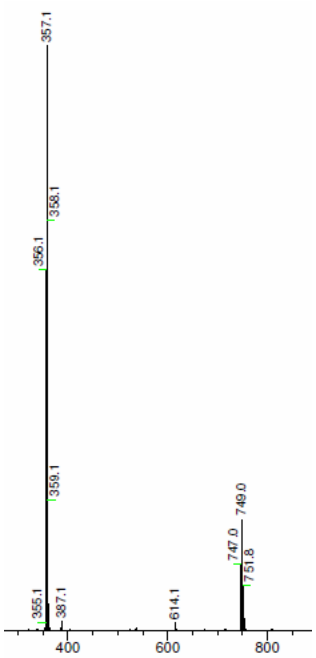

Figure AV.14. ESI-MS spectrum of the compound $[Cu^{II}_2(L^1SSL^1)Cl_4]$ dissolved in methanol. ESI-MS found (calcd) for ½ $[Cu^{II}(L^1SSL^1)Cl_4–2Cl]^+$ *m/z* 357.1 (357.4), $[Cu^{II}(L^1SSL^1)Cl_4–Cl]^+$; *m/z* 747.0 (747.0).

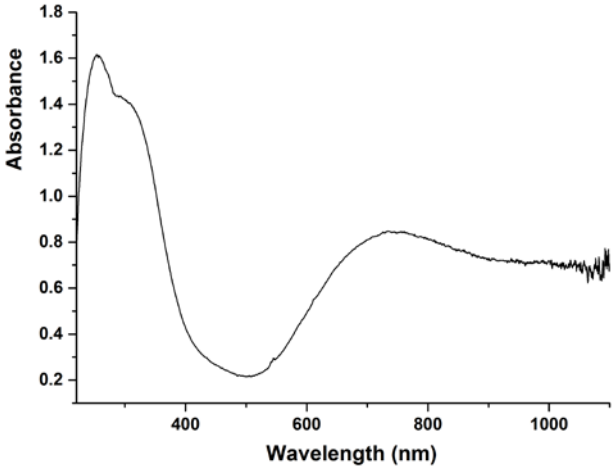

Figure AV.15. UV-vis spectrum of the compound $[Cu^{II}_2(L^1SSL^1)Cl_4]$ in the solid state.

Table AV.1. Crystallographic and structure refinement data of compounds $[Co^{II}(L^1SCH_3)Cl_2]$, $[Fe^{II}(L^1SCH_3)Cl_2]$ and $[Mn^{II}(L^1SCH_3)Cl_2]$.

	$[Co^{II}(L^1SCH_3)Cl_2]$	$[Fe^{II}(L^1SCH_3)Cl_2]$	$[Mn^{II}(L^1SCH_3)Cl_2]$
Chemical formula	$C_{15}H_{19}Cl_2CoN_3S$	$C_{15}H_{19}Cl_2FeN_3S$	$C_{15}H_{19}Cl_2MnN_3S$
M_r	403.22	400.14	399.23
Crystal system, space group	Monoclinic, *Cc*	Monoclinic, $P2_1/c$	Monoclinic, $P2_1/c$
Temperature (K)	110	110	110
a, *b*, *c* (Å)	11.2309 (3), 11.5965 (3), 13.6869 (3)	13.9394 (4), 8.3480 (2), 14.9559 (5)	14.0971 (3), 8.41155 (19), 14.9411 (3)
β (°)	101.207 (3)	90.723 (3)	91.435 (2)
V (Å^3)	1748.58 (8)	1740.22 (9)	1771.14 (7)
Z	4	4	4
Radiation type	Mo $K\alpha$	Mo $K\alpha$	Mo $K\alpha$
μ (mm^{-1})	1.41	1.29	1.16
Crystal size (mm)	0.35 × 0.18 × 0.15	0.40 × 0.38 × 0.23	0.50 × 0.32 × 0.22
Diffractometer	SuperNova, Dual, Cu at zero, Atlas	SuperNova, Dual, Cu at zero, Atlas	SuperNova, Dual, Cu at zero, Atlas
T_{min}, T_{max}	0.556, 1.000	0.463, 1.000	0.360, 1.000
No. of measured, independent and observed [$I > 2\sigma(I)$] reflections	13203, 4062, 3977	13654, 3988, 3525	16904, 4064, 3752
R_{int}	0.023	0.030	0.023
$(\sin\theta/\lambda)_{max}$ (Å^{-1})	0.653	0.650	0.650
$R[F^2 > 2\sigma(F^2)]$, $wR(F^2)$, S	0.020, 0.044, 1.04	0.029, 0.072, 1.05	0.022, 0.053, 1.03
No. of reflections	4062	3988	4064
No. of parameters	200	200	200
No. of restraints	2	-	-
H-atom treatment	H-atom parameters constrained	H-atom parameters constrained	H-atom parameters constrained
$\Delta\rho_{max}$, $\Delta\rho_{min}$ (e Å^{-3})	0.23, -0.19	0.56, -0.36	0.30, -0.24
Absolute structure parameter	0.011 (5)	n/a	n/a

Table AV.2. Crystallographic and structure refinement data of compounds $[Cu^{II}_2(L^1SSL^1)Cl_4]$ and $[Cu^{II}(L^1SCH_3)Cl_2]$.

	$[Cu^{II}_2(L^1SSL^1)Cl_4]$	$[Cu^{II}(L^1SCH_3)Cl_2]$
Chemical formula	$C_{28}H_{32}Cl_4Cu_2N_6S_2$	$C_{15}H_{19}Cl_2CuN_3S$
M_r	785.59	407.83
Crystal system, space group	Monoclinic, $P2_1$	Monoclinic, $P2_1/c$
Temperature (K)	110	110
a, b, c (Å)	9.28859 (17), 23.6394 (4), 14.6113 (2)	13.3848 (3), 8.60982 (16), 14.9420 (3)
β (°)	90.0369 (15)	90.3062 (18)
V (Å^3)	3208.30 (9)	1721.90 (6)
Z	4	4
Radiation type	Cu $K\alpha$	Mo $K\alpha$
μ (mm^{-1})	6.16	1.70
Crystal size (mm)	0.29 × 0.11 × 0.05	0.56 × 0.37 × 0.23
Diffractometer	SuperNova, Dual, Cu at zero, Atlas	SuperNova, Dual, Cu at zero, Atlas
T_{min}, T_{max}	0.373, 0.776	0.449, 1.000
No. of measured, independent and observed [$I > 2\sigma(I)$] reflections	22043, 10533, 10107	23663, 3959, 3762
R_{int}	0.028	0.024
$(\sin\theta/\lambda)_{max}$ (Å^{-1})	0.616	0.650
$R[F^2 > 2\sigma(F^2)]$, $wR(F^2)$, S	0.032, 0.083, 1.02	0.019, 0.049, 1.06
No. of reflections	10533	3959
No. of parameters	804	200
No. of restraints	131	
H-atom treatment	H-atom parameters constrained	H-atom parameters constrained
$\Delta\rho_{max}$, $\Delta\rho_{min}$ (e Å^{-3})	0.74, -0.58	0.36, -0.27